Validation of Finite Element Model of a Dish-Stirling System by Performing Experimental Modal Analysis

Master thesis in Applied Mechanics

ERIK KVARNSTRÖM
MALIN SETTERGREN

Department of Applied Mechanics, Division of Dynamics
CHALMERS UNIVERSITY OF TECHNOLOGY
Gothenburg, Sweden 2017

Master thesis 2017:15

Master thesis 2017:15

Validation of Finite Element Model of a Dish-Stirling System by Performing Experimental Modal Analysis

ERIK KVARNSTRÖM
MALIN SETTERGREN

Department of Applied Mechanics
Division of Dynamics
Chalmers University of Technology
Gothenburg, Sweden 2017

Validation of Finite Element Model of a Dish-Stirling System by Performing Experimental Modal Analysis

ERIK KVARSTRÖM
MALIN SETTERGREN

Supervisor: Hans Tolke, Uniso Technologies
Examiner: Peter Folkow, Chalmers University of Technology

Master Thesis 2017:15
ISSN 1652-8557
Department of Applied Mechanics
Division of Dynamics
Chalmers University of Technology
SE-412 96 Gothenburg
Sweden
Telephone +46 (0) 31 772 1000

Cover image: The figure shows the mounting of the test equipment onto the structure.

Chalmers Reproservice
Gothenburg, Sweden 2017

Acknowledgements

We would like to thank the following people who have contributed with knowledge and support during the project:
Thomas Abrahamsson, for advise and expertise in the area of experimental modal analysis. Our supervisor Hans Tolke for supporting us, and sharing his knowledge in Ansys Apdl. Roger Sjöqvist for constantly updating us on the project and giving practical ideas about the actual tests. Peter Folkow for report and project feedback. Kjell Jordansson for helping us during the first experiment day maneuvering the areal work platform and by doing so, making our tests that day possible.

Erik Kvarnström
Malin Settergren
Gothenburg, 9th June 2017

Validation of Finite Element Model of a Dish-Stirling System by Performing Experimental Modal Analysis

ERIK KVARNSTRÖM
MALIN SETTERGREN

Department of Applied Mechanics
Division of Dynamics
Chalmers University of Technology

Abstract

The energy consumption in the world is currently higher than ever before and it keeps rising. There is a fast rising demand for renewable energy sources such as solar power, and concentrated solar power systems can be a solution to this. However, in order to have robust systems that can compete with solar photovoltaic technologies, the life span and operational load effects on the structure need to be ensured. This can be done by using a validated finite element model. This thesis describes the experimental modal analysis and finite element analysis of a Dish-Stirling system developed by Cleanergy. The purpose of the thesis is to perform experiments on the structure to compare simulated results with actual tests, in order to validate that model in terms of dynamic response.

Testing on the structure was done in two different set-ups, one used for calibration and the other for validation. The structure was excited using a snap-back method, hanging a weight from the structure by a fishing line and burning the line to excite the structure. The structure was allowed to oscillate freely and eigenmodes were excited as the vibrations caused by the excitation were damped out. Data from experiments was processed and system identification of the response was done in the form of state space models. Eigenfrequencies and eigenmodes of the state space models were compared to eigenfrequencies and eigenmodes from the finite element model, which were found by performing modal analysis. Calibration of different parameters was done, changing one parameter at a time, and the calibrated data compared to the finite element results. The calibrated parameter which gave the best correlation between experiments and finite element model was used as input to the validation.

Due to the complexity of the model, only the first modes were used for the comparison, as the other modes were too complex, and had frequencies too close to each other to distinguish between them. Comparing the finite element model with the experiments showed that the experiments did manage to capture the eigenfrequencies of interest, however, when comparing the eigenvectors, there were differences in the correlation. Some modes were captured better than others. Calibration of the model led to a marginally better correlation. The validation confirmed the calibration, to some extent.

In conclusion, the finite element model corresponds well to the experiments, discrepancies in the results could be due to faults in experiment methodology, such as measurements were made too scarcely in the structure. It could also be due to a poorly calibrated finite element model. In order to further validate the finite element model more extensive experiments would need to be performed, as well as a more complex calibration procedure.

Keywords: Experimental modal analysis (EMA), Concentrated solar power (CSP), Finite element analysis (FEA), Modal Analysis, Vibration Testing, Signal processing

Nomenclature

Abbreviations

BNC	Bayonet Neill–Concelman
COMAC	Coordinate Modal Assurance Criterion
DAQ	Data Acquisition System
ECTS	European Credit Transfer System
EFI	Effective Independence
EMA	Experimental Modal Analysis
FEA	Finite Element Analysis
FE	Finite Element
FFT	Fast Fourier Transform
FRF	Frequency Response Function
MAC	Modal Assurance Criterion
CSP	Concentrated Solar Power
eCOMAC	Enhanced Coordinate Modal Assurance Criterion

Symbols

$\boldsymbol{\delta}$	Devation vector
$\mathcal{E}$	Expected value
$\mathcal{F}$	Fisher identification matrix
$\mathbf{\Gamma}$	Participation vector
λ	Eigenvalue
$\mathbf{\Lambda}$	Diagonal matrix with eigenvalues λ
n	Number of degrees of freedom
n_u	Number of outputs
n_y	Number of inputs
$\boldsymbol{\phi}$	Eigenvector
ν	Poisson's ratio
$\mathbf{\Phi}$	Column vector of eigenvectors $\boldsymbol{\phi}$
ρ	Density
$\mathbf{A}$	State matrix
$\mathbf{B}$	Input matrix
$\mathbf{C}$	Output matrix
$\mathbf{D}$	Feedthrough matrix
$\mathbf{E}_D$	Effective independence matrix
E	Young's Modulus
$\mathbf{F}_E$	Fractional eigenvalue distribution matrix
$\mathbf{F}$	External forces vector

$\mathbf{I}$	Identity matrix
$\mathbf{K}$	Stiffness matrix
L	Number of matching eigenvectors
m	Mass
$\mathbf{M}$	Mass matrix
$\mathbf{P}$	Transformation matrix
$\mathbf{q}$	Displacement
$\mathbf{Q}$	Deviation metric
$\mathbf{r}$	Influence vector
$\mathbf{R}$	Covariance matrix
$\mathbf{T}$	Correlation index matrix
$\mathbf{u}$	Excitation
$\mathbf{U}$	Distribution matrix
$\mathbf{V}$	Damping matrix
$\mathbf{x}$	State vector
$\mathbf{z}$	State vector

Subscripts

a	Acceleration
d	Displacement
eff	Effective
u	Input
y	Output
s	Candidate positions set
v	Velocity

Superscripts

A	Analytical
X	Experimental

Contents

List of Figures

List of Tables

1 Introduction

This chapter describes the background to the project, the problem statement that this thesis sets out to solve and the purpose for the problem. It also concerns the limitations of the project.

1.1 Background

Cleanergy is a Swedish based company developing a Dish-Stirling unit where a Stirling engine connected to a generator is positioned in the focal point of a solar concentrating reflective dish, effectively converting solar heat to electricity, see Figure 1.1. This electricity producing system is called Concentrated Solar Power, CSP.

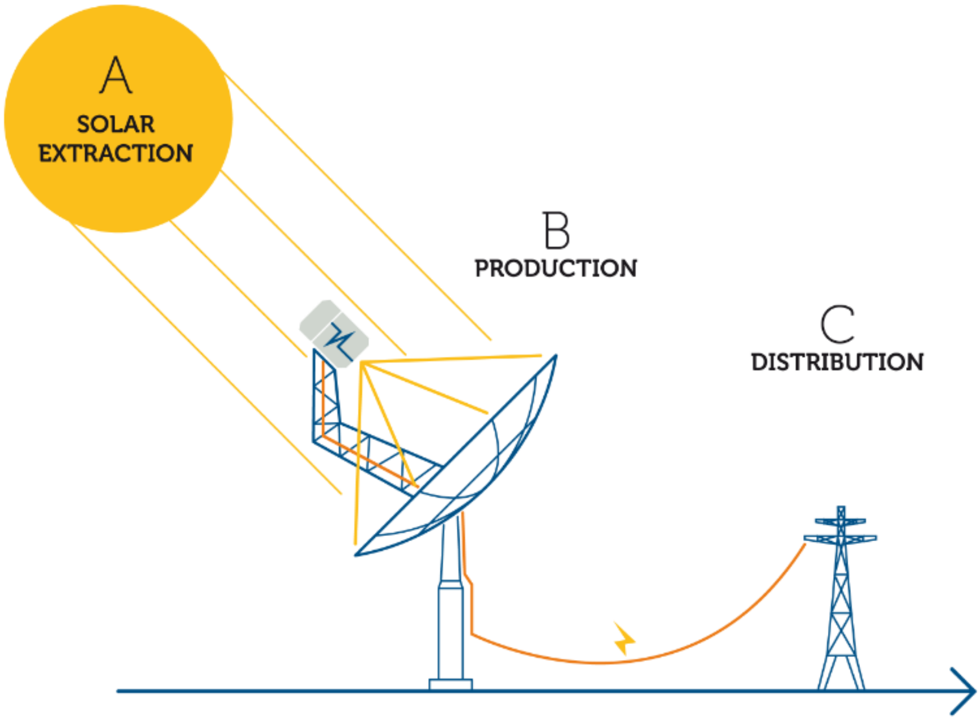

Figure 1.1: Cleanergy's electricity production system [1].

The unit is based on a Dish-Stirling system where a Stirling engine is mounted on a boom with a parabolic dish covered with mirrors on the opposite side. During the day, the dish tracks the sun and constantly concentrates the sunrays onto the Stirling engine, which generates electricity. The dish is built up of 11 individual sectors, each containing mirrors. The twelfth sector is empty in order to be able to maneuver the

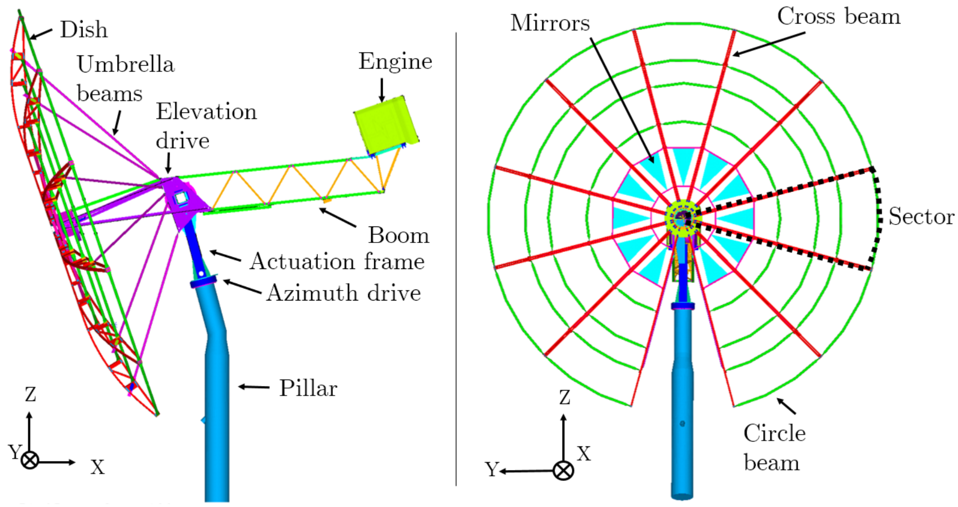

Figure 1.2: Principal sketch the full model, seen from the side and front.

dish in the elevation angle. Each sector has two cross beams on the sides and six circle beams where the mirrors are fastened, see Figure 1.2. Twelve umbrella beams are connected in between the sectors and to the housing of the elevation drive. The elevation drive and the azimuth drive enable movements in the elevation angle and azimuth angle, respectively. The drives are connected by an actuation frame, and the azimuth drive is connected to a concrete pillar.

The dish can be maneuvered in two directions, its position is described by the azimuth angle and the elevation angle, see Figure 1.3. A 0° elevation angle is when the engine is horizontal, and a 90° elevation angle is when the engine points upwards. A 0° azimuth angle is when the engine and pillar are pointing south, while a 180° azimuth angle means that the engine is pointing north.

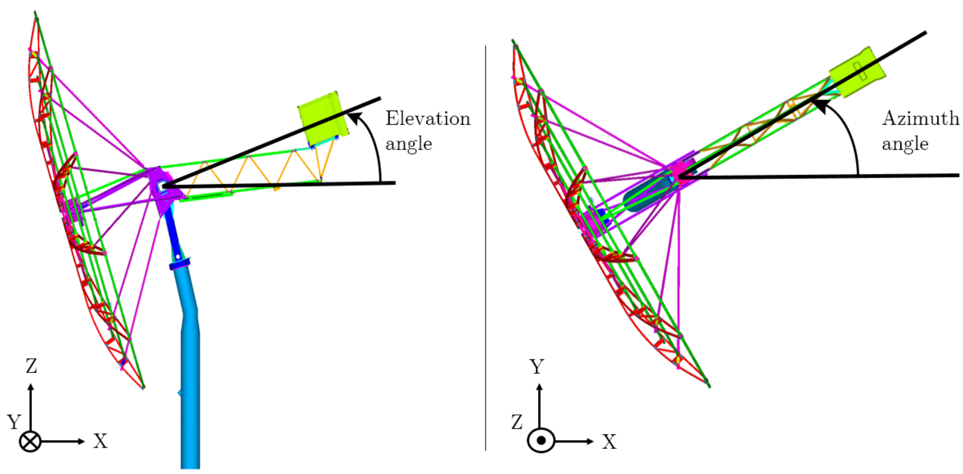

Figure 1.3: Elevation angle and azimuth angle for the Dish-Stirling system.

The structure is designed to operate optimally during quite windy conditions. For high wind speeds the dish is moved into safe position, with the side of the dish towards the wind.

The Stirling engine used by Cleanergy is of alpha type. This means that there are two cylinders, one expansion and one compression, with hydrogen gas flowing between the cylinders, see Figure 1.4. The sun beams hit the parabolic dish and the rays coincide in the focus point. At an offset from the focus point, a receiver is placed, in which hydrogen gas is heated. There is an offset because if the receiver would be placed in the focus point, it would become too hot. As the gas which flows in the receiver is heated, it requires more volume, which expands the expansion cylinder, causing the crankshaft to start to rotate. As the gas continues to heat, it expands even more, expanding into the compression cylinder. The compression cylinder is externally cooled, which lowers the pressure of the gas. This, in combination with the crankshaft momentum and the fact that both pistons are attached at the same point on the crankshaft, causes the expansion cylinder to upstroke. All the gas is now in the compression cylinder and the pressure drops even further due to cooling. As both cylinders have minimum volume, the cycle starts over again. The crankshaft is connected to a generator which converts the rotation into electricity.

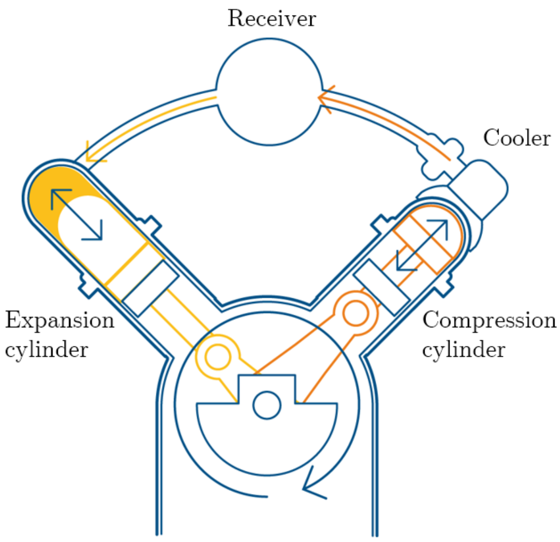

Figure 1.4: Principal sketch of Stirling alpha-type engine, [2].

The Stirling engine can be used at variable revolutions per minute, rpm, which, together with vibrations caused by the wind on the dish, creates a complex loading case. This complicates the calculation of the life span of the structure. The desired lifespan of the product is 25 years, however this is currently not verified.

Cleanergy currently has a finite element model, FE model, of the structure. To validate the analytical FE results, various tests on a full scale prototype is desired. This master thesis is focused towards establishing a good solid comparison between the dynamic response of the structure and the analytical results. As such, an important part is to understand the theoretical results, but also to perform the right test on the structure. Selecting the right tool such as measuring system as well as performing the test is crucial for the successful outcome of the FE model calibration.

1.2 Problem Statement

The problem to be solved during this master thesis is to perform vibration tests on the structure which will be used to calibrate and validate the FE model of the Dish-Stirling system.

1.3 Purpose

The energy consumption in the world is currently higher than ever before and it keeps rising. The prediction for the next 20 years, according to U.S. Energy Information Administration, is that this tendency will continue, [3]. There is a fast rising demand for renewable energy sources such as solar power, and the CSP system can be a solution to this. However, in order to have robust systems that can compete with solar photovoltaic technologies, the life span and operational load effects on the structure need to be ensured. This can be done by using a validated FE model.

1.4 Limitations

The experimental modal analysis will be performed on the boom and dish structure when it is mounted on the pillar which in turn is fixed to the ground, thus making it a pre-stressed modal analysis. Due to the design of the structure, different elevation and azimuth angles will have different eigenmodes, as the pre-stressed case is used. However, due to time limitations, in this thesis the azimuth angle will always be set to 180° and only a few set-ups of elevation angles will be considered.

In the FE analysis, FEA, an existing model from Cleanergy will be used with minor modifications and updates. Tests will be performed outdoors, and thus, the dish and boom are subjected to wind, however measures will be taken to minimise the effect of this, by e.g choosing the time of the tests.

Testing will only be done on one test object therefore there will be no evaluation of the spread that can be considered between test objects.

The project will be realised as a master thesis consisting of 30 European Credit Transfers credits, ECTS and will be done during the spring semester of 2017.

2 Theory

In this chapter the theory used in the project is described. First a basic theory behind structural dynamics systems is handled followed by theory on experimental modal analysis, including theory on signal processing. Lastly theory on comparing FEA and experimental modal analysis is described.

2.1 Structural Dynamics

A dynamic system can be described by the equation

$$\mathbf{M}\ddot{\mathbf{q}} + \mathbf{V}\dot{\mathbf{q}} + \mathbf{K}\mathbf{q} = \mathbf{F}, \tag{2.1}$$

with $\mathbf{M}$, $\mathbf{V}$ and $\mathbf{K} \in \mathbb{R}^{n \times n}$ denoting the mass, damping and stiffness matrix, for n points. The external forces are represented by $\mathbf{F} \in \mathbb{R}^{n \times 1}$, and the displacement, velocity and acceleration of the system is represented by $\mathbf{q}$, $\dot{\mathbf{q}}$, $\ddot{\mathbf{q}} \in \mathbb{R}^{n \times 1}$ [4]. Equation (2.1) is called the second order form of the equations of motion.

The first order form can be obtained by rewriting $\mathbf{q}$ and introducing a state vector $\mathbf{x} = [\mathbf{q}\ \dot{\mathbf{q}}]^{\mathrm{T}} \in \mathbb{R}^{2n \times 1}$, [4]. The external forces can be separated into components, $\mathbf{F} = \mathbf{U}\mathbf{u}$. Information about where the system is excited is described in the distribution matrix $\mathbf{U} \in \mathbb{R}^{n \times n_u}$, and $\mathbf{u} \in \mathbb{R}^{n_u \times 1}$ is the excitation for n_u inputs. Using this, Equation (2.1) can be rewritten as:

$$\begin{bmatrix} \mathbf{V} & \mathbf{M} \\ \mathbf{I} & \mathbf{0} \end{bmatrix} \begin{bmatrix} \dot{\mathbf{q}} \\ \ddot{\mathbf{q}} \end{bmatrix} + \begin{bmatrix} \mathbf{K} & \mathbf{0} \\ \mathbf{0} & -\mathbf{I} \end{bmatrix} \begin{bmatrix} \mathbf{q} \\ \dot{\mathbf{q}} \end{bmatrix} = \begin{bmatrix} \mathbf{U}\mathbf{u} \\ \mathbf{0} \end{bmatrix}, \tag{2.2}$$

with the lower equation being a dummy equation. Introducing the state vector $\mathbf{x}$ and rewriting gives:

$$\dot{\mathbf{x}} = \begin{bmatrix} \dot{\mathbf{q}} \\ \ddot{\mathbf{q}} \end{bmatrix} = -\begin{bmatrix} \mathbf{V} & \mathbf{M} \\ \mathbf{I} & \mathbf{0} \end{bmatrix}^{-1} \begin{bmatrix} \mathbf{K} & \mathbf{0} \\ \mathbf{0} & -\mathbf{I} \end{bmatrix} \mathbf{x} + \begin{bmatrix} \mathbf{V} & \mathbf{M} \\ \mathbf{I} & \mathbf{0} \end{bmatrix}^{-1} \begin{bmatrix} \mathbf{U}\mathbf{u} \\ \mathbf{0} \end{bmatrix} = \tag{2.3}$$

$$= \underbrace{-\begin{bmatrix} \mathbf{0} & -\mathbf{I} \\ \mathbf{M}^{-1}\mathbf{K} & \mathbf{M}^{-1}\mathbf{V} \end{bmatrix}}_{\mathbf{A}} \mathbf{x} + \underbrace{\begin{bmatrix} \mathbf{0} \\ \mathbf{M}^{-1}\mathbf{U} \end{bmatrix}}_{\mathbf{B}} \mathbf{u} = \tag{2.4}$$

$$= \mathbf{A}\mathbf{x} + \mathbf{B}\mathbf{u}, \tag{2.5}$$

with $\mathbf{A} \in \mathbb{R}^{2n \times 2n}$ being the state matrix and $\mathbf{B} \in \mathbb{R}^{2n \times n_u}$ the input matrix. The output of the system $\mathbf{y} \in \mathbb{R}^{n_y \times 1}$, is the response for n_y outputs. It is described differently depending on what output is desired, or measured:

$$\mathbf{y}_{\mathrm{d}} = \begin{bmatrix} \mathbf{P}_d & \mathbf{0} \end{bmatrix} \begin{bmatrix} \mathbf{q} \\ \dot{\mathbf{q}} \end{bmatrix} = \begin{bmatrix} \mathbf{P}_d & \mathbf{0} \end{bmatrix} \mathbf{x}, \quad \mathbf{y}_{\mathrm{v}} = \begin{bmatrix} \mathbf{0} & \mathbf{P}_v \end{bmatrix} \begin{bmatrix} \mathbf{q} \\ \dot{\mathbf{q}} \end{bmatrix} = \begin{bmatrix} \mathbf{0} & \mathbf{P}_v \end{bmatrix} \mathbf{x}, \tag{2.6}$$

with subscripts d and v denoting displacement and velocity respectively. $\mathbf{P}_d$ and $\mathbf{P}_v \in \mathbb{R}^{n_y \times n}$ describes the combined selection and transformation matrices for the respective output. If accelerations are measured, the following equation is needed:

$$\mathbf{y}_\mathrm{a} = \begin{bmatrix}\mathbf{0} & \mathbf{P}_\mathrm{a}\end{bmatrix} \begin{bmatrix}\dot{\mathbf{q}} \\ \ddot{\mathbf{q}}\end{bmatrix} = \begin{bmatrix}\mathbf{0} & \mathbf{P}_\mathrm{a}\end{bmatrix} \dot{\mathbf{x}} = \{(2.5)\} = \begin{bmatrix}\mathbf{0} & \mathbf{P}_\mathrm{a}\end{bmatrix} (\ \mathbf{A}\mathbf{x} + \mathbf{B}\mathbf{u}) = \tag{2.7}$$

$$= \begin{bmatrix}\mathbf{0} & \mathbf{P}_\mathrm{a}\end{bmatrix} \mathbf{A}\mathbf{x} + \begin{bmatrix}\mathbf{0} & \mathbf{P}_\mathrm{a}\end{bmatrix} \mathbf{B}\mathbf{u}, \tag{2.8}$$

for transformation matrix $\mathbf{P}_\mathrm{a} \in \mathbb{R}^{n_y \times n}$. In total, this means that the output can be described as, [4]:

$$\mathbf{y}(t) = \begin{bmatrix}\mathbf{y}_\mathrm{d} \\ \mathbf{y}_\mathrm{b} \\ \mathbf{y}_\mathrm{a}\end{bmatrix} = \underbrace{\begin{bmatrix}\begin{bmatrix}\mathbf{P}_\mathrm{d} & \mathbf{0} \\ \mathbf{0} & \mathbf{P}_\mathrm{v}\end{bmatrix} \\ \begin{bmatrix}\mathbf{0} & \mathbf{P}_\mathrm{a}\end{bmatrix} \mathbf{A}\end{bmatrix}}_{\mathbf{C}} \mathbf{x} + \underbrace{\begin{bmatrix}\mathbf{0} \\ \mathbf{0} \\ \begin{bmatrix}\mathbf{0} & \mathbf{P}_\mathrm{a}\end{bmatrix} \mathbf{B}\end{bmatrix}}_{\mathbf{D}} \mathbf{u} = \tag{2.9}$$

$$= \mathbf{C}\mathbf{x} + \mathbf{D}\mathbf{u}, \tag{2.10}$$

with $\mathbf{C} \in \mathbb{R}^{n_y \times 2n}$ representing where the output is measured, also called the output matrix, and $\mathbf{D} \in \mathbb{R}^{n_y \times n_u}$, the feedthrough matrix, how the output is directly affected by the excitation. Matrices $\mathbf{C}$ and $\mathbf{D}$ are different depending on what type of output is measured, which can be seen in Equation (2.9). Equations (2.5) and (2.10) describe the full state space representation, also called the first order form.

If there is no excitation, i.e. $\mathbf{u} = \mathbf{0}$, the system can be said to be free, and Equation (2.5) becomes $\dot{\mathbf{x}} = \mathbf{A}\mathbf{x}$. As the eigenvalue problem is the solution to the free system, studying Equation (2.5) the eigenvalue problem for the states $\mathbf{x}$ becomes, see [4]:

$$\mathbf{A}\boldsymbol{\Phi} = \boldsymbol{\Phi}\boldsymbol{\Lambda}, \tag{2.11}$$

with $\boldsymbol{\Phi}$ being the eigenvectors ordered in the columns in a matrix and $\boldsymbol{\Lambda}$ the eigenvalues in a diagonal matrix. In order to decouple Equations (2.5) and (2.10) a similarity transformation from states $\mathbf{x}$ to states $\mathbf{z}$, where $\mathbf{x} = \boldsymbol{\Phi}\mathbf{z}$ can be done. This leads to Equation (2.5) becoming:

$$\boldsymbol{\Phi}\dot{\mathbf{z}} = \mathbf{A}\boldsymbol{\Phi}\mathbf{z} + \mathbf{B}\mathbf{u}, \qquad \text{multiply by } \boldsymbol{\Phi}^{-1} \tag{2.12}$$

$$\boldsymbol{\Phi}^{-1}\boldsymbol{\Phi}\dot{\mathbf{z}} = \boldsymbol{\Phi}^{-1}\mathbf{A}\boldsymbol{\Phi}\mathbf{z} + \boldsymbol{\Phi}^{-1}\mathbf{B}\mathbf{u} = \{Eq.(2.11)\} \tag{2.13}$$

$$\dot{\mathbf{z}} = \boldsymbol{\Lambda}\mathbf{z} + \boldsymbol{\Phi}^{-1}\mathbf{B}\mathbf{u}. \tag{2.14}$$

The output signal $\mathbf{y}$, Equation (2.10) becomes:

$$\mathbf{y} = \underbrace{\mathbf{C}\boldsymbol{\Phi}}_{\overline{\mathbf{C}}} \mathbf{z} + \mathbf{D}\mathbf{u}, \tag{2.15}$$

where $\overline{\mathbf{C}}$ is the eigenvector matrix associated with the output signal, since it contains the eigenvectors for the states, by use of the eigenvector matrix $\boldsymbol{\Phi}$. $\overline{\mathbf{C}}$ also contains information about how the sensors affect the output in output matrix $\mathbf{C}$. In order to correctly compare the eigenvectors from the FE model, these are the eigenvectors used for the comparison, as they are associated with the measured response.

In order to calculate the importance of each mode, the modal participation factor and effective modal mass can be calculated. The modal participation factor and effective mass can rate how important each mode is. If a full modal analysis is to be done for a complex structure, the effective mass or the modal participation factor can be an effective method to determined the modes that participate the most to the overall movement of the structure, [5]. For a 3D-model, the effective mass and modal participation factor is calculated in all six degrees of freedom, i.e. translation in all three global axes rotation around the three global axes. The effective mass can be interpreted as the mass that is exposed to forces and the modal participation factor as how much movement there is in each mode relative to all modes. For the system in (2.1), the eigenvectors are stored in the column matrix $\mathbf{\Phi}$. The generalised mass matrix of the system can then be calculated as, [6]:

$$\hat{\mathbf{m}} = \mathbf{\Phi}^{\mathrm{T}}\mathbf{M}\mathbf{\Phi}. \tag{2.16}$$

If the eigenvectors have been normalised, the generalised mass matrix is the identity matrix. An influence vector $\mathbf{r}$ can be defined as the resulting displacement of mass elements from static application of a unit ground displacement, [5]. The influence vector cause rigid body motion in all modes. Using this, the modal participation factor Γ for mode i is obtained as, [5]:

$$\Gamma_i = \frac{\left(\mathbf{\Phi}^{\mathrm{T}}\mathbf{M}\mathbf{r}\right)_i}{\hat{m}_{ii}} \tag{2.17}$$

and the effective mass m_{eff} for each mode i is:

$$m_{\text{eff},i} = \frac{\left(\mathbf{\Phi}^{\mathrm{T}}\mathbf{M}\mathbf{r}\right)_i^2}{\hat{m}_{ii}}. \tag{2.18}$$

2.2 Experimental Modal Analysis

A modal analysis consists of describing a structure in terms of its natural characteristics, that is frequency, damping and mode shapes, [7]. Understanding the characteristics can help to understand how the structure behaves, and can be used to validate an FE model. In order to compare a physical product with an FE model, an experimental modal analysis, EMA, can be performed. This is done by finding the actual modes of the structure by experiments, and can be compared with the calculated modes from FEA. If the FE model and experiments do not coincide, a calibration can be necessary. A calibration can be done on parameters, such as stiffnesses and thicknesses, but also on boundary conditions and modelling of joints. As there is always an uncertainty in testing, it is best to perform several tests on the same test object, and preferably several tests on multiple test objects, to account for the variance between them.

2.2.1 Performing Tests

There are several aspects involved in performing tests. This involves choosing a suitable method and proper equipment depending on test conditions and test object.

2.2.1.1 Equipment

EMA is commonly done using sensors, namely accelerometers. An accelerometer is a kind of transducer that transforms kinetic energy into an electrical signal. For the most common accelerometer, the Piezoelectric accelerometer, this is done in accordance with the piezoelectric effect which states that an applied strain generates an electrical charge, [8]. This is done by using a piezoelectric crystal assembled together with a mass inside the accelerometer. Acceleration of the measured item loads the mass with a counter force which loads the crystal. The load creates a proportional strain which generates an electric charge, the output signal. There are two types of Piezoelectrical accelerometers, *charge mode accelerometers* and *voltage mode accelerometers* (or integrated electronic piezoelectric accelerometers, IEPEA) [4].

Charge mode accelerometers need external measurement electronics [4]. Since they operate on lower voltage they are much more sensitive to the surrounding environment and require well isolated cables which should be as short as possible. There are special cables available that should be used which have been treated with for example lubricating graphite in order to exclude noise effects. The output electrical charge signal is of high impedance and needs to be transformed with an external charge amplifier into a low impedance voltage signal, which is more appropriate for measurements applications. Further precautions that are required are to keep the transducers, cables and connectors clean and dry in order to secure high insulation resistance. Voltage mode accelerometers consist of internal measurement electronics which are provided with electrical power through a coaxial cable. The internal measurements generate an output signal of low impedance which is insensitive to noisy electromagnetic surroundings and cable lengths. Hence, the voltage mode accelerometers are the most common and easiest to use. The primary area of use for charge mode accelerometers are for very high temperature measurements, where the internal electronics of the voltage mode accelerometer fail [4].

One of the most popular accelerometer is the triaxial accelerometer, TRIAX. TRIAX looks like a dice, with five smooth sides and the cable connection at the last side. All the smooth sides can be used as the mounting side. It is connected only with one cable which is very beneficial compared to other models which have up to four connected wires. These accelerometers can if necessary be made very small and still maintain accuracy. There are also uniaxial accelerometers which only measure the acceleration along one axis. The uniaxial accelerometers can also be dice-shaped and thus measure in any direction, albeit only one at a time. They can also be flatter to reduce their weight. The uniaxial accelerometer is often sufficient since it is enough to capture the deflection of the modes, [4].

Three parameters to consider when choosing accelerometer are mass, sensitivity and dynamic range, [9]. Since the vibration of the considered structure is dependent on its mass, the outcome could change if additional mass is added. Hence, if the considered structure is of light weight, a lightweight accelerometer is needed. The general rule is that the accelerometer should not weigh more then 10 % of the vibrating structure. For larger structures, the accelerometer mass has a negligible impact, since the accelerometers are so light compared to the structure itself. Larger accelerometers generally have better accuracy than smaller accelerometers. However, sensitivity is often not a problem, since small accelerometers often have sufficient sensitivity. Likewise, the dynamic range is seldom a problem, apart from when abnormally low or high accelerations are measured. The lower limit for what is measurable is where the acceleration can not be separated from noise. This is usually at around 0.01 m/s^2. The upper limit is often of interest when measuring mechanical shocks and is determined from the structural strength of the accelerometer. Usually an accelerometer can handle accelerations up to 50–100 km/s^2.

The mounting of the accelerometers is of great importance, especially for measuring higher frequencies. The surface where the accelerometer is mounted should be flat and clean, in order to not influence the result. The accelerometers can be mounted with a threaded stud or with thin layers of beeswax or silicone grease. With clean surfaces, acceleration levels of up to 100 m/s^2 are measurable when beeswax is used for mounting the accelerometer, [9].

One important issue to have in mind is the effect of the eigenfrequencies of the accelerometer itself. The accelerometer should never be used to measure frequencies approaching or higher than the first natural frequency of the accelerometer. The rule of the thumb is to use the accelerometer only for frequencies up to 33 % of its first natural frequency. This critical frequency is usually around 20–30 kHz for standard accelerometers, but can be as high as 180 kHz for very small ones. The specific value for each accelerometer is determined by the manufacturer through testing.

The usual connector for the uniaxial accelerometers is the BNC (Bayonet Neill–Concelman) connector. It is a bayonet style connector used for coaxial cables with a locking mechanism. A coaxial cable has a cylindrical conductor with cylindrical insulation on both sides. Within the inner insulation there is one additional conductor. BNC cables most commonly exist with either an impedance of 50 Ω or 75 Ω. The higher impedance cable is often used for data acquisition since the attenuation is low, [10].

2.2.1.2 Test Types

There are different types of tests that can be performed, all exciting a test object in different ways. The most precise excitation method is to use a shaker. The shaker works by applying a load by moving a rod via a load transducer which should add as little mass as possible. The force is applied via a rod which should apply the force horizontally without exciting the test object in a longitudinal direction or creating bending or torsional couplings. There are several types of shakers within different ranges, and the type of shaker used depends on the size of the test object. Two common types of modes of signals from a shaker is full cycle excitation mode and burst excitation mode, [4]. The full cycle mode means that there is a signal the entire period, while a burst mode means that there is a signal in the beginning of the period, and that the signal source then is quiet for the rest of the period. The duration of the burst period is usually decided so that the response in the test object has died down at the end of the period, minimising the risk of leakage, see section 2.2.2.5. The signal can then be of, usually, random or chirp kind. The chirp signal means that the frequency is continuously varied several times during the sampling while the random signal means that the frequency is varied randomly, and can in some cases be just noise. For the full period mode, this means that there is a high risk of leakage, as the signal might not be periodic. Figure 2.1 shows two examples of burst mode signals, both the chirp and random.

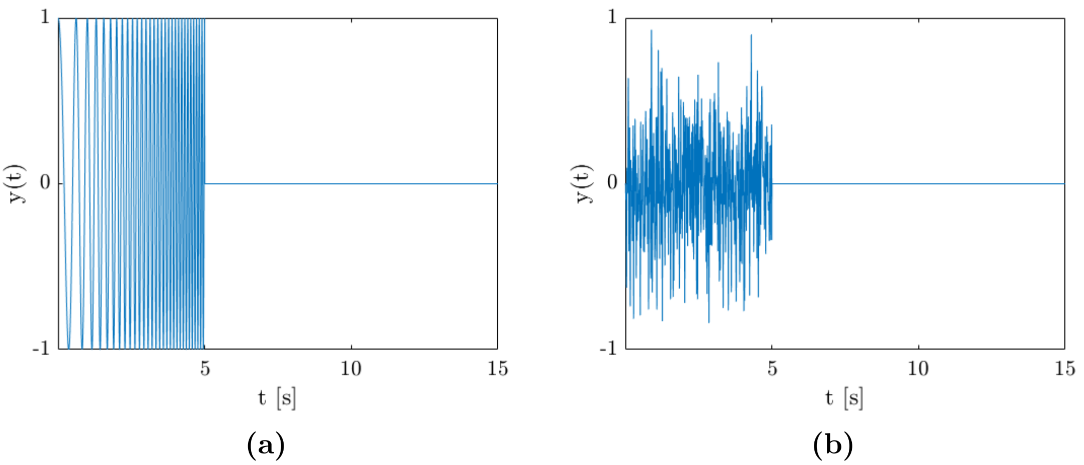

Figure 2.1: (a) Burst mode chirp signal with sweep from 1 to 5 Hz for 5 s, (b) Filtered burst mode random signal, [4].

An impact test is done by aperiodically exciting a test object, using e.g. a hammer. The hammer has a load transducer at the tip to measure the load applied, [4]. Due to the nature of the application of the force, the impact test is less accurate than a shaker test, as it can be difficult to repeat the test with the exact same excitation, i.e. hammer hit. For small test objects, usually a rubber sticker is placed where the hammer should hit, both so that the same spot is hit for several tests, but also to avoid missing to hit the specimen perfectly normal to the surface with the hammer, but that the force is instead distributed through the rubber sticker.

Another excitation is the snap-back test. It consists of applying a stress to the test object, e.g. by suspending a known weight at a point, and then releasing it. This gives a known excitation force, the gravity pulling on the weight, and as the vibrations after the release from pre-stressed state are damped out by the test object, the eigenfrequencies are passed and can thus be measured. This type of test has a very good repeatability, and is suitable for complex structures and conditions.

Apart from EMA, other tests can also be performed, in order to validate an FE model. A paper from National Solar Thermal Test Facility (NSTTF) described performing static loading tests on a heliostat to use as validation of FE model, [11]. A heliostat is a structure with mirrors mounted to create a plane surface and directing sun beams towards a target, such as a sun tower. The test was done by applying loads at points on the structure. The response from the static test was measured using lasers and transducers, or ”string potentiometers”. The measured response can then be compared to the response from the FE model and the model can thereby be calibrated and validated.

2.2.1.3 Boundary Conditions

In order to be able to perform the modal analysis, the boundary conditions need to be taken into account. The boundary conditions in the FE model should match those that are used in tests. The structure can be tested in free test conditions, meaning that it is not attached to the ground, [4]. This is of course impossible to achieve fully, but can be mimicked by suspending the test object in using e.g. light elastic bands, or springs or by placing it on e.g. foam or special purpose airbags. The free conditions means that the rigid body modes will be visible in the analysis. These modes occur at 0 Hz, but as the test object is influenced by the suspension, the rigid body frequencies will be a little higher. Depending on the suspension, damping can be introduced that is not present in the totally free state.

The test object can also be tested in grounded conditions, for test objects too large and cumbersome to be mounted with free support. The grounded condition is easier to achieve in the FE modelling stage, by simply locking degrees of freedom. However, it is more difficult to achieve in reality, due to the fact that the ground is never completely still. To account for this, the movement of the ground base can be measured as well as the test object, to assure that the mobility of the ground is at least much less than the mobility of the test object.

2.2.1.4 Placement of Accelerometers

It is important to mount the sensors, usually the accelerometers, and actuators, where the system is excited in order to correctly observe the behaviour of the system. The worst positions to place all sensors is at the nodes of the modes as the behaviour of the structure cannot be seen at the node, as it does not appear to be moving there, [4].

Method of Effective Independence, EFI

To calculate the most optimal placement of the sensors, there are methods that can be used. A commonly used method is the method of effective independence, developed by Kammer, [12]. The method is based on ranking each candidate position based on how much it contributes to the linear independence of the modes that are to be observed. Thus, the nodes with the least contribution can be removed and the ranking is updated iteratively until the desired number of sensors is reached. The candidate positions are those positions where it is physically possible to place sensors, as some nodes can be internal or difficult to reach. The candidate set should also be large enough to capture the physical behaviour of the structure in the modes that are interesting.

Assuming that the measured displacement response at the candidate positions $\mathbf{y}_s$ can be written as:

$$\mathbf{y}_s(t) = \mathbf{\Phi}_s \mathbf{z}(t) + \mathbf{v}(t), \tag{2.19}$$

with $\mathbf{z}(t)$ being the generalised structural motion, $\mathbf{v}(t)$ being the measurement noise and $\mathbf{\Phi}_s$ being the truncated modal matrix of the finite element model pertaining only to candidate positions and directions and the modes of interest, [4]. Assuming also that the measurement noise is stationary, that is roughly the same in all points and during the entire test, the covariance matrix describing the variance between the points, $\mathbf{R} \equiv \mathcal{E}\left[(\mathbf{z}-\hat{\mathbf{z}})(\mathbf{z}-\hat{\mathbf{z}})^T)\right]$ should be minimised according to Kammer [12]. Here $\hat{\mathbf{z}}(t)$ is the target states, or estimate, the true system is $\mathbf{z}$, and $\mathcal{E}$ denotes the expected value, see [13]. The target states should be as close to the true states as possible, meaning that the determinant of $\mathcal{F} = \mathbf{R}^{-1}$ should be as large as possible. The measurement noise can be characterised by the variance σ^2 as the statistical properties are identical in each sensor, and the measurement noise is not correlated between the sensors, [4]. This means that:

$$\mathbf{R}^{-1} = \mathcal{F} = \frac{1}{\sigma^2}\mathbf{\Phi}_s^{\mathrm{T}}\mathbf{\Phi}_s = \frac{1}{\sigma}\mathcal{F}_s, \tag{2.20}$$

with $\mathcal{F}$ being the Fisher information matrix, and $\mathcal{F}_s$ the scaled matrix. In order to study how the Fisher matrix is maximised, the determinant is used as a scalar measure. The contribution, the effective independence index vector $\mathbf{E}_D$, of each sensor i is then defined as:

$$\mathbf{E}_D^i = \frac{\det(\mathcal{F}) - \det(\mathcal{F}^i)}{\det(\mathcal{F})}, \tag{2.21}$$

with $\mathcal{F}^i$ denoting the Fisher information matrix, i.e. the inverse of the covariance matrix, when the i-th sensor is removed. The sensor which gives the least decrease in the determinant is then removed.

In order to simplify calculations, and not have to calculate all determinants separately, an effective method was devised by Kammer, [12]. In this method the eigenvalue problem is solved:

$$[\mathcal{F}_s - \mathbf{\Lambda}\mathbf{I}]\mathbf{\Phi} = 0, \tag{2.22}$$

with $\mathbf{\Lambda}$ being the eigenvalues and $\mathbf{\Phi}$ the eigenvectors ordered in a matrix. The effective independence matrix can then be formed as:

$$\mathbf{F}_E = [\mathbf{\Phi}_s\mathbf{\Phi}] \otimes [\mathbf{\Phi}_s\mathbf{\Phi}]\mathbf{\Lambda}^{-1}. \tag{2.23}$$

The term $\mathbf{F}_{E,ij}$ corresponds to the i-th sensor location's contribution to j-th eigenvalue, and the matrix $\mathbf{F}_E$ denotes the fractional eigenvalue distribution. Addition of the terms in each row will result in a column matrix $\mathbf{E}_D$, see Equation (2.21). The entry with the lowest contribution can then be removed iteratively until the desired number of sensors is reached.

There are suggestions in an article by Friswell et al. that when the number of sensors are higher than the number of modes, the EFI tends to cluster sensors, at least for plates and beams, [14]. Friswell et al. indicates that as the EFI method is iterative, meaning that only one accelerometer is removed in each iteration, an optimal set is not found when only the worst accelerometer is removed, thus EFI is not effective. It is instead suggested that a first cut of candidate nodes should be made using an exhaustive search. That is testing all possible combinations of sensors for each number of desired sensors in the end, and thus removing the worst sensor, and then adding sensors to see which gives the best result. The article also suggests that the use of the determinant of the Fisher matrix is a poor choice to see the independence in the modes. It appears to be a good measurement in the extreme points, that is when the modes are linearly dependent and orthonormal. Friswell et al. states that there is no direct correlation between linear independence and the determinant between these extremes. The article suggests that the condition number of the mode shape matrix is a good estimate for linear independence. Using this measure suggests that the EFI is a poor method when the number of sensors used is higher than the number of modes. However, an exhaustive search takes more time, especially for more complex structures, and the Fisher determinant has been shown to be a good measure in most situations, [4].

Other methods than the EFI are also proposed, modifying it by placing sensor where the strain energy is the highest, [15]. Another method uses the kinetic energy as a measure for optimisation, with the updating in the same way as the EFI, [16].

2.2.1.5 Placement of Actuator

When deciding where to excite the test object, it is important that the modes are excited by the actuator. This can be done by looking at the modes of interest from FE modelling, and seeing in which nodes there is movement for all modes of interest, so as to not excite the specimen in a node. The node of a mode is a point where the system does not move i.e. is fixed. If you want to suppress a mode, a good excitation point can be in a node of that mode. Depending on which type of test is done, the displacement in the correct direction is of interest. If a shaker or impact test is done, the force is usually applied normal to the surface, so this is the direction of interest. If a snap-back test is done using weights, this means that the vertical displacement is of interest.

2.2.2 Signal Processing

In practice, the response from a structure is measured by sensors which convert the physical response into electrical signals [4]. The electrical signal is then converted in a data acquisition system, DAQ. The DAQ samples the continuous signal at a sampling frequency. The signal can then be exported to for example Matlab for further signal processing. Signal processing consists going from raw signal to a state space model where desired data has been extracted. When recording signals it is common that noise, which is unwanted disturbance in the response, appears. Part of signal processing is to decrease the influence of noise, which can be done by aliasing and averaging, as well as by applying filters or windows.

2.2.2.1 Aliasing

The response from a structure is obtained as analog signals, which are continuous in the time domain. However, when measuring the response, it needs to be converted to a discrete time domain. During such discretization, if the sampling frequency is too low, high-frequency components can be misinterpreted as low-frequency contributions, see Figure 2.2, [4]. The high frequency signal, 9 Hz shown in red, is sampled at 10 samples per second. This means that the signal can be interpreted as a 1 Hz signal in blue, as can be seen in the figure. High frequencies are generally unwanted as they can generally be interpreted as noise. The solution to aliasing is to use an anti-aliasing filter which remove any high frequency signals by means of a low pass filter, which only lets low frequencies through, and creating a modified signal to be discretized. The cut-off frequency for the filter, that is the cut-off when only lower frequencies will be allowed to pass, can be calculated. An anti-aliasing filter is applied in the DAQ.

2.2.2.2 Aligning

If tests which are aperiodic are performed, a periodicity can be created by repeating a test several times, creating blocks. These blocks need to be aligned to each other so that they appear to start at the same time thus creating a periodic response. This is done by stepwise moving one block and comparing it to the others at each stage, in accordance to the algorithm, [17]:

$$\hat{T}_{xy}(m) = \begin{cases} \sum\limits_{n=0}^{N-m-1} x_{(n+m)} y_n^* & \mathrm{m} \geq 0 \\ \hat{T}_{xy}^*(-m), & \mathrm{m} < 0, \end{cases}$$

where x_n and y_n are the same place, e.g. the drop, at two different blocks and m is the step. For each step m, the value $x_{(n+m)}y_n^*$ at each position for the two considered blocks is calculated and added to the sum for that step. The total sum is $\hat{T}_{xy}$. This is done again, where one block has been offset by one step at a time. When $\hat{T}_{xy}$ is maximised, the correlation between the two blocks is largest and that delay of the offset block is m. Using the delay, the blocks can be aligned.

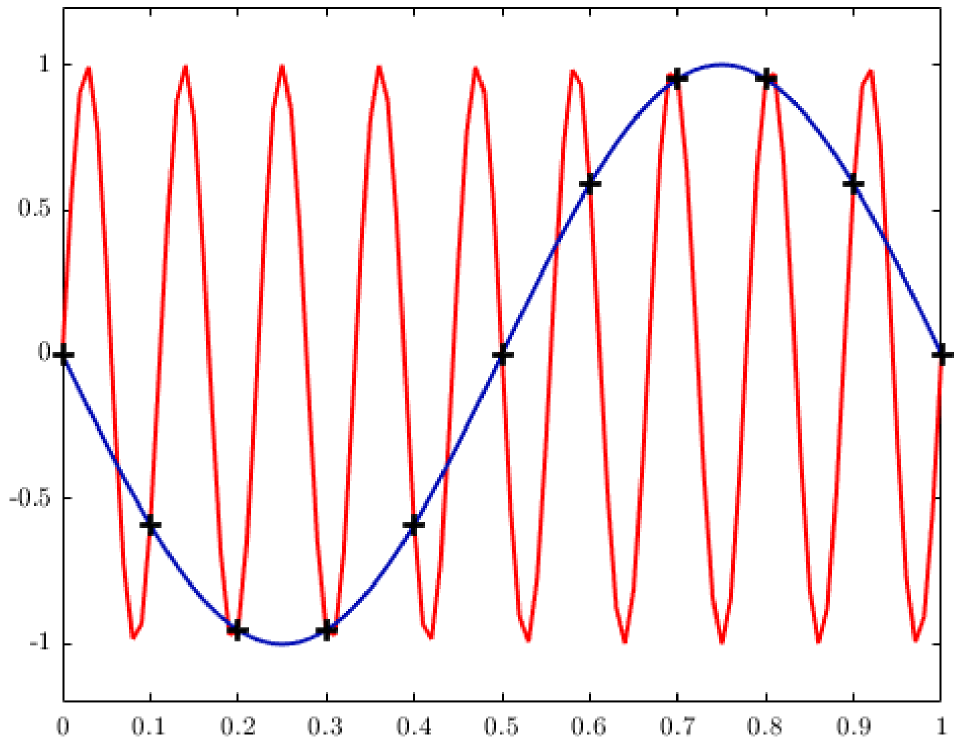

Figure 2.2: Sampling a high-frequency signal, (red), at points, (black) aliasing it as a low frequency signal (blue).

2.2.2.3 Linear Averaging

In order to eliminate the influence of noise in the signal analysis, linear averaging can be used. Linear averaging is when several signals which are nominally similar, but contain variations are summarised to decrease the impact of the variations. In practice, this can be done for when the excitation is repeatedly used and measured thus creating time blocks. As the periodic part of the response will always be the same, the noise will not. All time blocks are then summarised and divided by the number of time blocks. Hence, the noise has been distinguished and decreased through averaging, [18].

2.2.2.4 Filters

A filter is a tool used to change the features of a signal by removing unwanted components. For example, this can be to reduce background noise by suppressing certain frequencies, [4]. Different filters are designed to operate at different frequency ranges. Low-pass filters attenuate high frequencies while a high-pass filter attenuates the lower frequencies. Band-pass filter attenuates both low and high frequencies and only let a certain frequency range in between through. The accuracy of a filter is described by its order which is the level of its approximating polynomial. In signal processing, one of the most commonly used filters is the Butterworth filter. It has a very flat frequency response over the non filtered range. This means it has a very low impact on the frequencies that are not subjected to filtering. The Butterworth filter and other filters are seen in Figure 2.3, where the flat frequency response of the Butterworth filter can be seen compared to the other filters for the non filtered range. Figure 2.4 shows Butterworth filters of different orders and also the ideal response where frequencies over a certain frequency limit are removed completely. Filtering can be applied in the time domain and the frequency domain, but is more easily seen in the frequency domain [4].

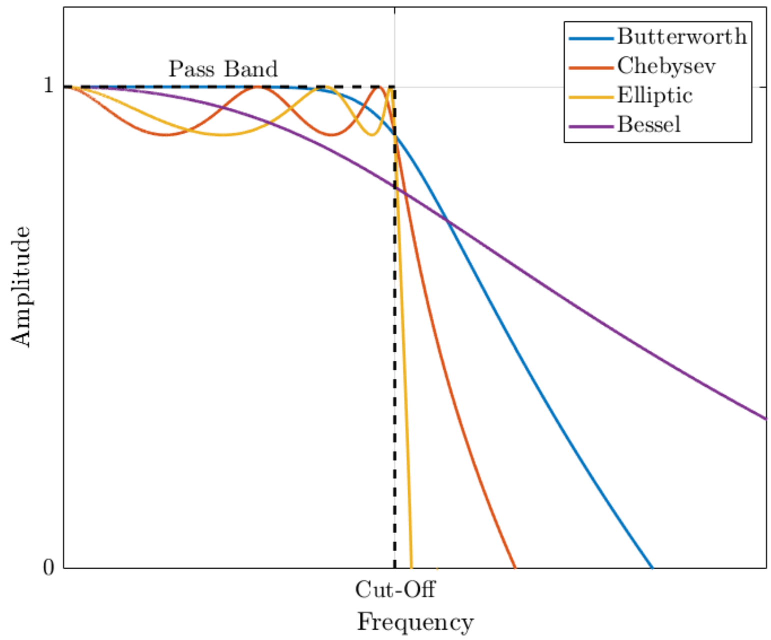

Figure 2.3: Different filters commonly used in signal processing, [19].

2.2.2.5 Frequency Response Function, FRF

A first step of an EMA is to create a function that relates the excitation, input, to the response, output of the system. This is called a Frequency response function, FRF. The FRF is the ratio of output to applied force on a structure and it can be obtained by simultaneously measuring an applied force as well as the response in the structure, [4]. The response can be measured as displacement, velocity or acceleration depending on the equipment. The data is obtained as functions, one function for how each measuring point depends on each excitation point. This data is obtained as signals in the time domain, and using a Fast Fourier Transform, FFT they can be transferred to complex numbers the frequency domain. These complex numbers can then be separated as a magnitude and a phase, making up the FRF. The FFT is based on a periodic assumption, that the signal repeats itself with a certain period. During the FFT, it is possible that leakage occurs.

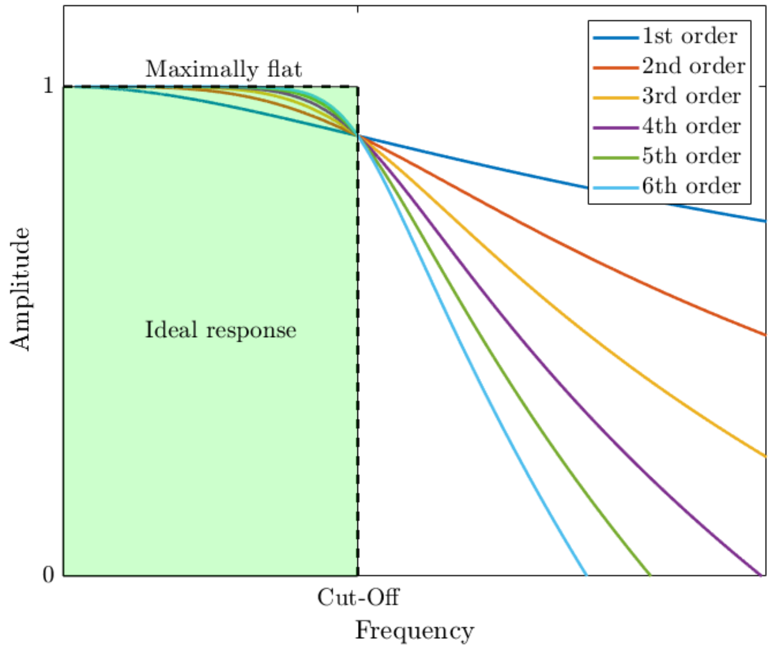

Figure 2.4: Butterworth filters of different orders, [19].

Leakage

Leakage is data that is lost when transforming the signal from the time domain to the frequency domain, when using FFT. This occurs because only a limited time history is considered together with the periodicity assumption in the FFT, [4]. When a perfectly periodic time history is transformed, Figure 2.5a, the frequency response is clear and definite, Figure 2.5c. However, when this is not the case and there is discontinuity in the time-history, Figure 2.5b, the frequency response suffers from leakage, Figure 2.5d. More specifically, this means that the frequency response no longer shows a consistent response, but the signal energy has rather ”leaked” over the frequency spectra. Hence, leakage is a serious problem in signal analysis.

To avoid leakage, different methods for making the time history periodic can be applied. Methods such as changing the length of the time history or adding zeros at the ends of the time history to make it periodic can be used. However, the most common used method is probably windows. The idea of windowing is to change the signal before performing the FFT to make the time history more periodic, [4, 7]. This is done by adding a weighted function, a window, to the time history. Different windows have different purposes, applying no window can be likened to applying a uniform window, see Figure 2.6a. For continuous signals, Hanning or Cosine Taper windows are commonly used, see Figure 2.6b and c. For transient vibration applications exponential windows are preferred, as there is a lot of information in the beginning of the time record, see Figure 2.6d, [20]. In general it can be concluded that the use of windows impair the result and the response will appear overrated regarding damping, but it is an improvement if leakage is the alternative or if the signal is too affected by irregular noise, [4, 7].

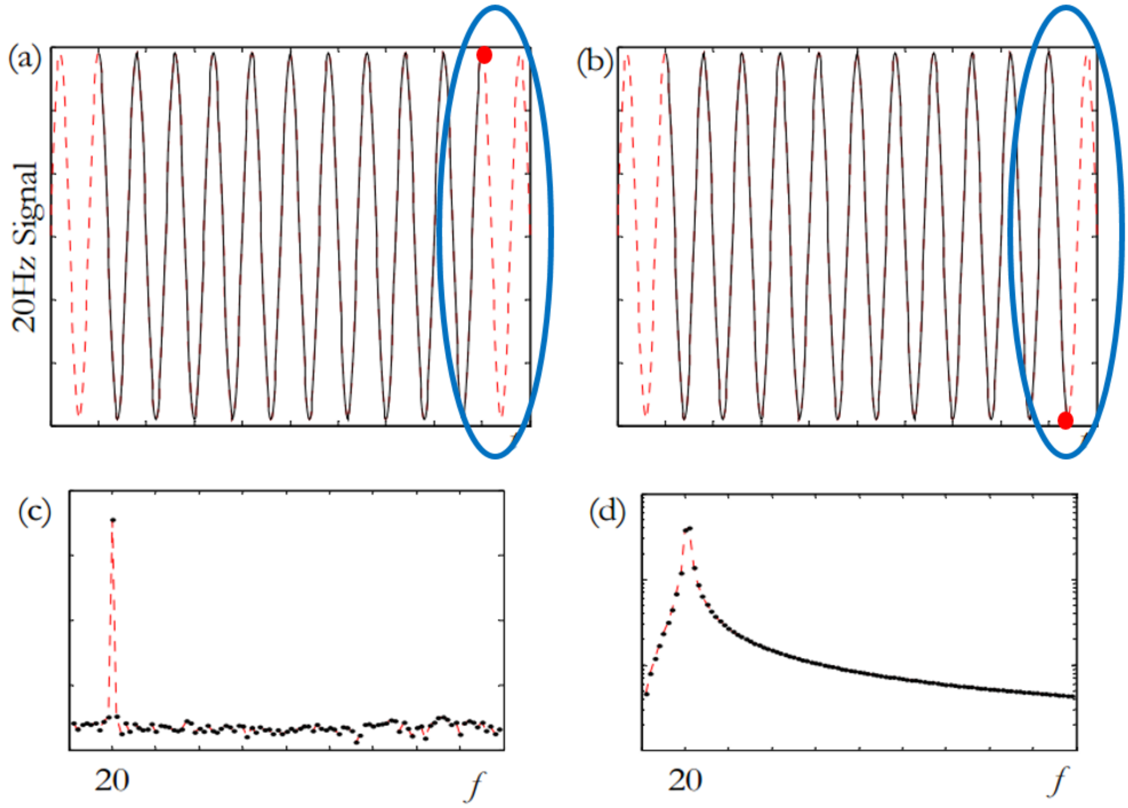

Figure 2.5: The red dot in the blue circle notes in (a) and (b) where the signal is cut, creating a time history. A periodic (a) and a non-periodic(b) time history is considered. (a) results in a clear frequency response(c) while (b) suffers from leakage (d), [4].

2.2.2.6 System Identification

As the FRF is calculated, some parameters of the system need to be identified, in order to describe the system as Equations (2.5) and (2.10), i.e. by a mathematical mode. Using the mathematical model, eigenvectors and eigenfrequencies can be calculated for comparison with the FEA. The system identification is usually done as a state space identification of the FRF. A commonly used algorithm for this is the N4SID algorithm, [4].

The first step in the N4SID algorithm is to establish the block Hankel matrices, as described by Abrahamsson, [4], for the output, input and combined input/output with the given input and output from the FRF. This just means ordering the data so that the ascending skew-diagonal from left to right is constant, e.g. for the output, $\mathbf{u}$:

$$\begin{bmatrix} u_0 & u_1 & u_2 & \cdots \\ u_1 & u_2 & u_3 & \cdots \\ u_2 & u_3 & u_4 & \cdots \\ \vdots & \vdots & \vdots & \ddots \end{bmatrix}. \tag{2.24}$$

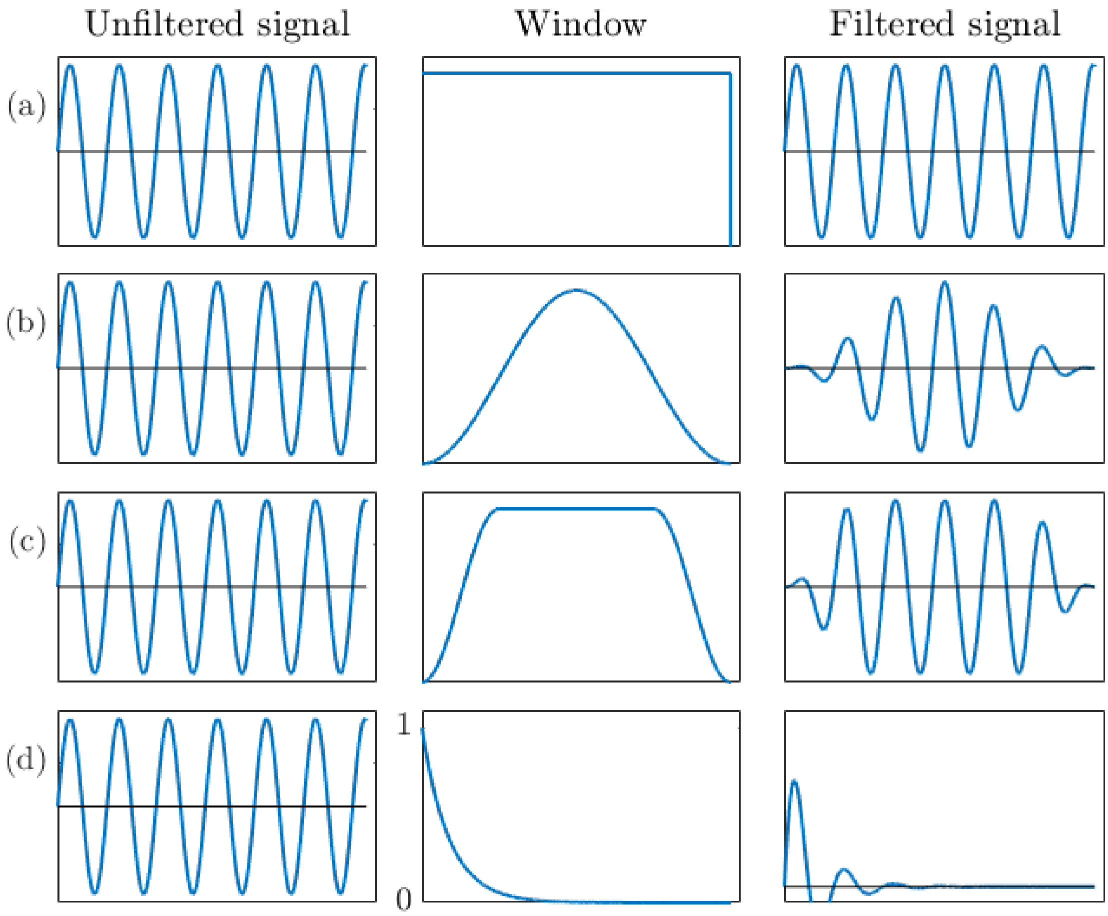

Figure 2.6: Uniform (a), Hanning (b), Consine Taper (c) and exponential (d) windows, [20].

The Hankel matrices can be subdivided into a past and a future part, where the first i rows pertain to the past, for a total of $2i-1$ entries, depending on the sampling interval. From this, the projected future outputs, $\tilde{\mathbf{Y}}_f$ can be calculated as the oblique projection on the row space of the combined past input/output Hankel matrix $\mathbf{W}_p$, of the future output Hankel matrix, $\mathbf{Y}_f$ along the row space of the future input Hankel matrix $\mathbf{U}_f$, i.e. $\tilde{\mathbf{Y}}_f = \text{proj}(\mathbf{Y}_f, \mathbf{W}_p, \mathbf{U}_f)$. The oblique projection can be described by Figure 2.7, but for $\text{proj}(\mathbf{M}_\alpha, \mathbf{M}_\gamma, \mathbf{M}_\beta)$ in the 2-dimensional space. Figure 2.7 also shows the orthogonal projection for comparison.

The next step is to calculate the singular value decomposition of $\tilde{\mathbf{Y}}_f$, i.e. to factorise the matrix, and to use these factors to calculate the observability matrix, $\mathcal{O}^X$. The observability matrix for experimental data is defined as:

$$\mathcal{O}^X = \begin{bmatrix} \mathbf{C} \\ \mathbf{CA} \\ \vdots \\ \mathbf{CA}^{i-1} \end{bmatrix}, \quad i > n. \tag{2.25}$$

with $\mathbf{A}$ and $\mathbf{C}$-matrices from Equations (2.5) and (2.10). The observability of a system is described as how well states of a system can be determined by registering

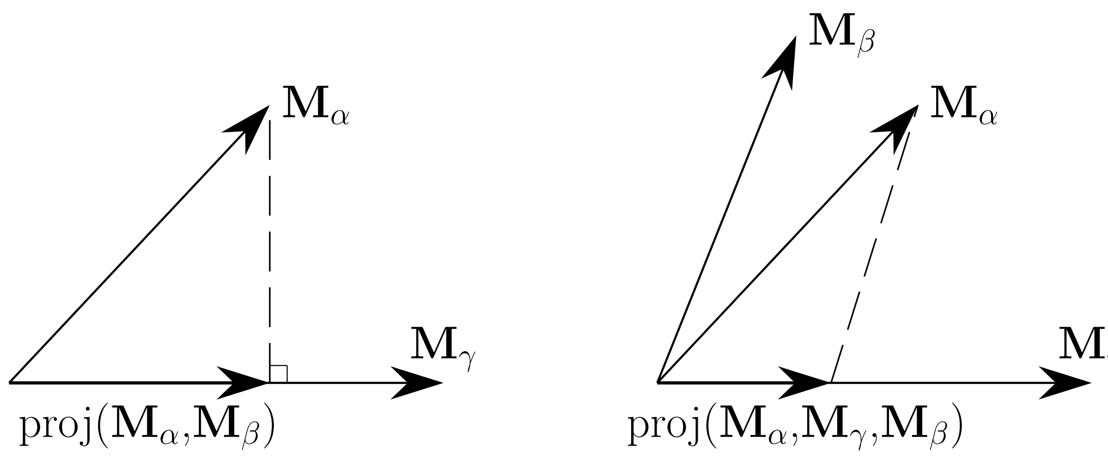

(a) **(b)**

Figure 2.7: (a) Orthogonal projection of $\mathbf{M}_\alpha$ on $\mathbf{M}_\beta$. (b) Oblique projection of $\mathbf{M}_\alpha$ on $\mathbf{M}_\gamma$ in direction of $\mathbf{M}_\beta$, [4].

the output of the system, [4]. It can be seen from Equation (2.25) that the **C**-matrix in the state space representation is the first part of the observability matrix. Denoting the first $i-2$ rows of the observability matrix $\overline{\mathcal{O}}^X$ and the last $i-2$ rows of the matrix $\underline{\mathcal{O}}^X$, the **A**-matrix can be found by:

$$\mathbf{A} = (\overline{\mathcal{O}}^X)^\dagger \underline{\mathcal{O}}^X \tag{2.26}$$

with † denoting the pseudo-inverse, see [21]. With **A** and **C** known, the problem is linear in **B** and **D** for the discretized time realisation, see [4]:

$$\mathbf{x}_{k+1} = \mathbf{A}\mathbf{x}_k + \mathbf{B}\mathbf{u}_k \tag{2.27}$$

$$\mathbf{y}_k = \mathbf{C}\mathbf{x}_k + \mathbf{D}\mathbf{u}_k, \tag{2.28}$$

with k representing the time step. Ordering the values in **y**, **B** and **D** into column vectors, **Y**, $\tilde{\mathbf{B}}$ and $\tilde{\mathbf{D}}$, the following can be written:

$$\mathbf{Y} = \mathbf{\Gamma} \begin{Bmatrix} \tilde{\mathbf{B}} \\ \tilde{\mathbf{D}} \end{Bmatrix}. \tag{2.29}$$

$\mathbf{\Gamma}$ is an influence matrix which is found by simulating the response contribution for unit elements in $\tilde{\mathbf{B}}$ and $\tilde{\mathbf{D}}$ respectively. The elements in **B** and **D** can be found by solving for $\tilde{\mathbf{B}}$ and $\tilde{\mathbf{D}}$:

$$\begin{Bmatrix} \tilde{\mathbf{B}} \\ \tilde{\mathbf{D}} \end{Bmatrix} = \mathbf{\Gamma}^\dagger \mathbf{Y}. \tag{2.30}$$

With matrices **A**, **B**, **C** and **D** found, the state space model in Equations (2.5) and (2.10) can be constructed. From the state space model, as can be seen in Equation (2.11), the eigenvectors and eigenfrequencies can be calculated in the measurement points.

When constructing the state space model, the order is of importance. The order describes how well the equations describe the FRF. However, as some noise is incorporated in the FRF a too high model order means some peaks due to noise in the FRF is interpreted as eigenfrequencies.

2.3 Comparing Finite Element and Experiments

When an EMA has been done, the obtained resonance frequencies can be compared to the eigenvectors and eigenvalues obtained from modal analysis in the FE model.

2.3.1 Modal Assurance Criterion

The Modal Assurance Criterion, MAC, can be used to analyse if two modes obtained from different methods really are the same mode, by observing the eigenvectors. By using the MAC method and only consider eigenvectors, only the shapes of the eigenmodes can be determined. Hence, the amplitude of the eigenmodes remain unknown. MAC is a correlation coefficient that in fact describes the angle between two modal vectors and is calculated as:

$$MAC(i,j) = \frac{((\boldsymbol{\phi}^{(i)X})^T \boldsymbol{\phi}^{(j)A})^2}{(|\boldsymbol{\phi}^{(i)X}||\boldsymbol{\phi}^{(j)A}|)^2} \tag{2.31}$$

where $\boldsymbol{\phi}^X$ is the eigenvectors obtained from the experimental modal testing and $\boldsymbol{\phi}^A$ is the eigenvectors obtained from the FE model that correspond to the locations of the accelerometers in the experimental tests. In Equation (2.31) the superscripts i and j denote different eigenvectors. If MAC is equal to 1, the angle between the modal vectors is zero and they are the same mode. However, MAC values up to 0.8 can be seen as sufficiently good correlations. If the modes are orthogonal the MAC value is 0 and there is no correlation at all, [22].

2.3.2 COMAC and eCOMAC

In order to test how each accelerometer contributes to how similar the modes are, a Coordinate Modal Assurance Criterion, COMAC, can be calculated, [23]. The COMAC method is based on performing an initial comparison between eigenvectors from experiment and FEA, using e.g. the MAC method. The L eigenvectors that make up matching pairs, $\boldsymbol{\phi}_r^A$ and $\boldsymbol{\phi}_r^X$, are normalised and compared to see how each sensor contributes to a low MAC number. The COMAC number for each sensor q, can be calculated as:

$$COMAC(q) = \frac{\sum_{r=1}^{L} |\phi_{qr}^A \phi_{qr}^X|^2}{\sum_{r=1}^{L} \left({\phi_{qr}^A}^2\right) \sum_{r=1}^{L} \left({\phi_{qr}^X}^2\right)} \tag{2.32}$$

The sensors with a COMAC number far from zero indicates an experimental error for that sensor, [4].

An extended method of comparing the eigenvectors is to use the Enhanced coordinate modal assurance criterion, [23]. The eCOMAC method tackles the issue of calibration scaling errors and sensor orientation mistakes, by normalising the eigenvectors that form pairs so that they are of unit length. One of the eigenvectors is then multiplied with a complex number of unit length, so the eigenvector is unchanged in space, but so that the difference between the matching eigenvectors is minimised. After that the eCOMAC number for each sensor can be calculated as follows, from [4]:

$$eCOMAC(q) = \frac{1}{2L} \left\| \hat{\boldsymbol{\phi}}_q^X - \hat{\boldsymbol{\phi}}_q^A \right\| \tag{2.33}$$

with L being the number of eigenpairs that match, and $\hat{\boldsymbol{\phi}}_q^X$ and $\hat{\boldsymbol{\phi}}_q^A$ the modified eigenvector values for a specific sensor q.

2.3.3 Calibration

When the models are compared, a calibration can be done to achieve a better fit between models. This means that parameters are identified which can be tuned within a specified range and the fit between the models is reevaluated. The calibration is done on parameters in the FE model, as a good EMA is already representing reality. By changing material parameters, entries in the mass and stiffness matrices in Equation (2.1) are changed. Calibrating a model can be done using software, such as the Matlab app FEMcali, [24]. The app uses Nastran, Matlab, Abaqus or StructDyn as a solver for the FEA. In FEMcali calibration is done using the Latin Hypercube sampling which ensures that a near random sampling occurs, and can also account for variables that are uniformly or normally distributed, see [4]. A quadratic deviation metric, Q, is then used to compare how the model changes with the parameters stored in vector $\mathbf{p}$:

$$\begin{aligned} Q(\mathbf{p}) &= \boldsymbol{\delta}^T(\mathbf{p})\boldsymbol{\delta}(\mathbf{p}) \\ \boldsymbol{\delta}(\mathbf{p}) &= \mathbf{z}^A(\mathbf{p}) - \mathbf{z}^X \end{aligned}$$

where $\mathbf{z}^X$ and $\mathbf{z}^A$ is the output from experiments and FEA respectively. The calibrated parameters are then those that minimise Q, with the search direction $\Delta\boldsymbol{p}$.

2.3.4 Validation

Validation of a model is done to ensure that the model fulfills a purpose. If the model is to be used to answer certain questions, the model should be validated to answer these questions, [4]. A calibration can be done on some test data to see which parameters need to be changed in order for the model to fit well. Other test data should then be used for validation of the calibration to ensure that the calibration is generally valid, and not just valid for the one calibration test object.

3 Method

The method used for the project is described in this chapter. Firstly the FEA process is described, followed by the experimental method and lastly the method of comparing the two types of analyses.

3.1 Finite Element Analysis

In the FEA an FE model constructed by Cleanergy was used, see Figure 1.2, and all analyses were done in the software Ansys Apdl. The FE model is simplified, for example all mirrors are only represented by mass elements at the attachment points. Only the inner mirrors are additionally represented by shell elements for visualisation. The model was modified to include a more detailed sub-model of the engine as well as a toolbox on the beams between the elevation drive and the dish. For the modelling, the boundary condition at the bottom of the pillar was set to fixed. In reality the pillar is molded onto a concrete ground plate.

As the dish system can be rotated by its azimuth and elevation drive, it was important to decide which set-up to do the tests on. This is because the set-ups are affected differently by gravity, and thus the pre-stressed modal solutions become different. Therefore FEAs were done on several different set-ups, see Table 3.1. The angles were chosen to represent different realistic operating scenarios. This was done so that different scenarios could be investigated, both with regards to conditions during testing which at the time were uncertain, and the importance of each set-up, depending on how often it occurred during use.

Table 3.1: Set-ups considered in FEA.

Elevation	**Azimuth**
90°	-180°
-70°	-180°
0°	-180°

For all these test an initial modal analysis was performed to observe the mode shapes. It could be seen that the same initial modes appeared for all configurations, for example the first mode was a rotation of the dish, while the second and third were a bending in the elevation axis, both up-and-down and side-to-side. After that there were differences in the exact order and uniqueness of the modes, which were mainly due to gravity affecting the set-ups differently.

Candidate positions for the accelerometers were chosen where there appeared to be a lot of movement in the structure, and to be spread out evenly on these parts. For example several modes were observed where the cross beams of adjoining sectors were moving both in- and out-of-phase, and thus candidate positions were chosen on both cross beams. The candidate positions were chosen on the circle beams, cross beams and umbrella beams as well as the boom, and all positions were in the form of elements. No candidate elements were chosen on the pillar, elevation drive, azimuth drive or the actuation frame as there appear to be little movement there on most modes. The mirrors were also ruled out as possible places for mounting the accelerometers on, as this could compromise their critical alignment. In total 277 candidate positions were chosen. As the structure moves in a complex manner, the movement along all three local axes was chosen as possible candidates. This made the total number of candidate positions 831 with each direction in the candidate element considered a candidate element in its own, as only uniaxial accelerometers were available. The same candidate positions were chosen for all set-ups. All candidate positions can be seen in Figure 3.1, where it can be seen that the candidate positions form a simplified model of the structure.

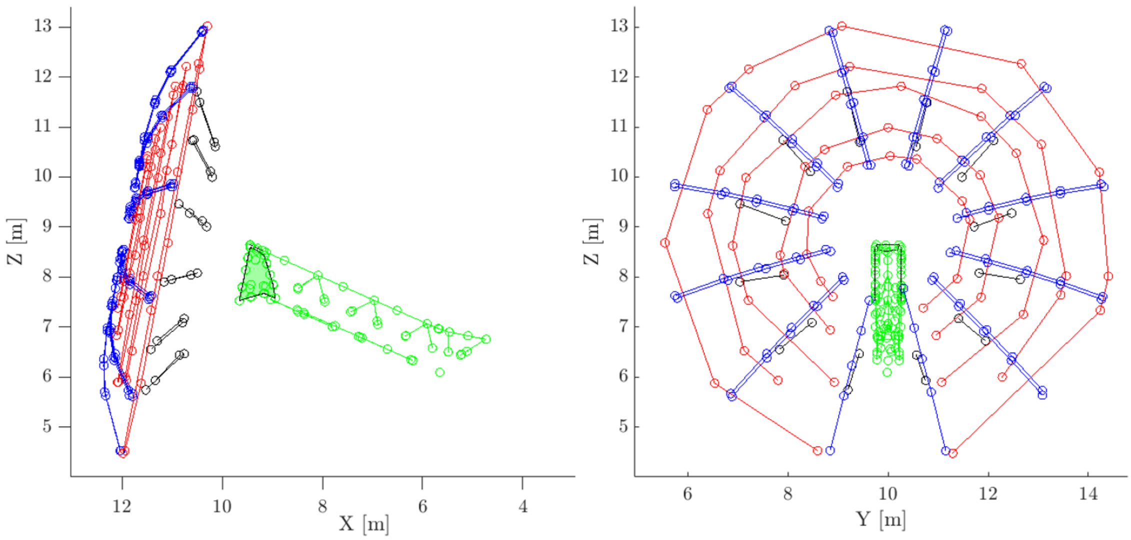

Figure 3.1: Candidate positions in the structure, from the side and front.

As the eigenmodes were to be compared, the eigenvectors of the candidate positions needed to be calculated and extracted from the FEA. Accelerometers measure the response in the local coordinate system, i.e. relative to the surface where it is placed. Therefore local coordinate systems had to be created in the FE model for the candidate positions. The coordinate systems were constructed by firstly finding the normal vector to the candidate element. This was done by laying surface elements on top of the desired elements, as only the surface elements contain information about the normal vector in Ansys Apdl. This outward normal vector is used as the x-direction in the local coordinate system. The positive normal direction had to be manually checked for each element in order to be outward from the surface. A node in a specified direction is then used as the y-direction. This is so that the direction can be identified when performing the tests, so that the same directions are compared in FEA and EMA. For the most part, this direction was along the beam in question, e.g. towards the fringe of the dish, in the case of the cross beams, and towards the engine, in the case of the boom. These directions then make up the local coordinate system for each candidate element, with the origin in the center of the element. In the local coordinate system, the eigenvector for each mode can be calculated from the FEA for each candidate element.

The analyses were done for modes up to 50 Hz, which in all set-ups corresponded to around 225 modes. The upper limit of 50 Hz was used as modes under 50 Hz are considered to possibly be excited by the engine or the wind. The engine can run up to 2500 rpm, which is around 40 Hz, whereby the upper limit of 50 Hz including a safety margin is set by Cleanergy to avoid large global modes under this limit. As for the lower limit, it was chosen to be just above 0 Hz. The engine has a idle speed of 800 rpm, which corresponds to a frequency of roughly 13 Hz. However, the structure can also be excited by the wind, which is considered to have a low frequency range, whereby the lower limit of just above 0 Hz was chosen.

3.2 Experimental Modal Analysis

The method pertaining to EMA can be divided into three main parts. Firstly the tests are planned to ensure that what is desired is achieved by the tests. Secondly, the tests are performed and lastly the signal obtained is processed.

3.2.1 Test Planning

The test was chosen to be carried out as a snap-back test. This test method was used because it was a good way to excite the complex structure and still ensure a good repeatability of the test. By using a different actuator, such as an impact hammer, this would have been difficult to achieve. A good repeatability was important to be able to perform linear averaging and reduce impact from the wind. The equipment used in the experiments was from Chalmers University of Technology, and consisted of four uniaxial voltage mode accelerometers and a signal toolbox, see Table 3.2. For each test set, one accelerometer was placed where the load was applied, while the other three were moved around to different locations for each set. The locations were determined by EFI out of the candidate positions, see Figure 3.1.

3.2.1.1 Determining of Accelerometer Positions

The results from the FE modelling, the eigenvectors for the candidate elements for the modes up to 50 Hz, were exported to Matlab, where further data processing was done. In order to find the best positions for the accelerometers during the tests, EFI was implemented, see section 2.2.1.4. To determine which modes were considered important, the effective mass was used as a tool. The effective mass was used because the modes that were considered interesting were those where a lot of the structure was moving, the global modes. The modes of individual beams for example are not considered to be as detrimental to the structure as the global modes, and it is thus

Table 3.2: List of Equipment.

Item	Specification
Computer	
Signal Toolbox	
Data Acquisition System	QuickDAQ
4 Accelerometers	Uniaxial
4 Cables	BNC
4 Extension Cables	BNC, 75 Ω
4 Joints	BNC
Beeswax	
Water Carrier	10 kg
Gavia Fishing Line	Braided
Storm Lighter	
Duct Tape	
Hooks	

not as important to validate the FE model for these modes. For each set-up, possible modes of interest were looked at, both to include those with the most effective mass, and also the first modes, as these have the lowest frequencies and are therefore most likely excited by the wind. The lower modes were also chosen as these are the fundamental modes and the frequencies were spread further apart.

The eigenvectors for all candidate positions for the modes of interest were used as input in the EFI, and from that, accelerometer positions that would be good were calculated. A possible excitation point was chosen from the calculated accelerometer positions, by both considering which positions were practically possible to hang a weight from and by looking at the eigenmodes. Positions for the excitation with a large value in the eigenmode in the downward direction for certain modes, indicates that those modes would be easily excited in that excitation point. Using this technique, the modes of interest could be decided, see Table 3.3. Most of the considered modes were only excited in one of the set-ups. However, mode eleven was excited in both set-ups and mode ten in neither of them.

In order to be able to differentiate the modes, the number of positions used would have to be at least the number of interesting modes. As the numbers of accelerometers and the time available were limiting factors, different amounts of accelerometers positions were investigated to account for different scenarios.

The EFI was then used to find the important candidate positions. The article by Friswell et al., [14] suggests that in order to avoid clustering, see section 2.2.1.4, the amount of accelerometers used for the test should be the same as the amount of

Table 3.3: Modes excited at each set-up during test.

	Excited at set-up	
Mode	**-70°**	**0°**
1		X
2	X	
3		X
4	X	
5		X
6	X	
7	X	
8		X
9	X	
10		
11	X	X
50		X
67	X	
68	X	
75	X	

modes of interest. However, the article also states that this is mainly a problem for plates and beams, and not for complex structures. This was investigated by choosing few modes of interest and using EFI to calculate more positions for accelerometers than the number of modes. The EFI showed that there was little or no clustering, whereby clustering was not considered a problem for this type of structure. The positions calculated by the EFI for 6 accelerometer positions for the 0° set-up can be seen in Figure 3.2. As can be seen in the figure, the accelerometers are quite evenly spread which indicates that the result from the EFI is plausible. Figure 3.3 shows the 13 accelerometer positions calculated by EFI for the -70° set-up.

3.2.1.2 Test Plan

A test plan was made in order to estimate the duration of the tests and make the test procedure efficient. The estimated time needed for the tests was calculated by estimating the time for the different stages in the test procedure and summarising. Different test plans were made for different possible test scenarios after the required time was calculated. For each set-up, the number of accelerometer positions should be as many as possible in order to capture more of the dynamic response. The considered number of positions that were reasonable due to the time consumption were determined to be 7, 10, 13 and 16 positions, and therefore different test plans

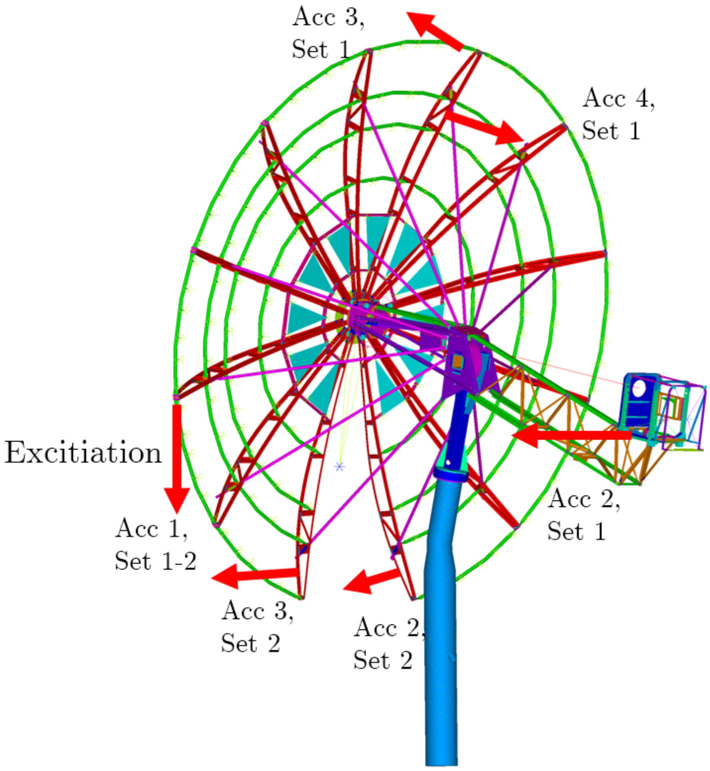

Figure 3.2: The accelerometer positions for the 0° set-up chosen by EFI and used in tests for this set-up.

were made depending on which scenario would be done during the testing. Looking at the accelerometer positions chosen by the EFI and comparing these between the set-ups, finding accelerometer positions that could be used for both tests were important for time saving reasons. In the case where the same direction was chosen from the EFI, but on adjacent circle beams in the same sector for example, a common circle beam was chosen to be used in both set-ups. The test plan also included a description of the most efficient way of relocating the accelerometers, in order to limit the time used by an aerial work platform used to position the accelerometers.

3.2.1.3 Pre-Test

In order to try out the test procedure, a pre-test was made at Chalmers. The test object was a small composite wind turbine blade and for the testing, the same hardware and software that were to be used for the tests on the Dish-Stirling system were used. For the pre-test the same testing procedure i.e. a snap-back test was implemented, and the tests were repeated several times. The signal acquired was then processed and Matlab scripts for this were developed, that were to be used for the Dish-Stirling tests. Performing the pre-test meant that the Dish-Stirling test could be planned more carefully and the signal processing prepared more thoroughly.

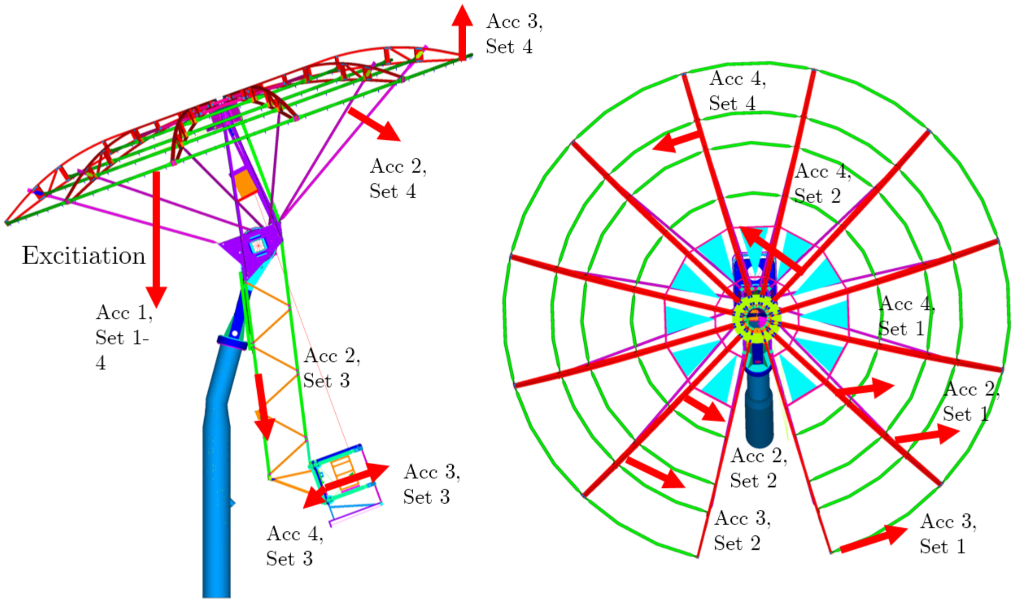

Figure 3.3: The accelerometer positions for the -70° set-up chosen by EFI and used in tests for this set-up.

3.2.2 Test Execution

The tests were performed on Cleanergy's most recent prototype in Åmål, Sweden on the 19th and 20th of April. The software QuickDAQ was used for data acquisition, [25]. Since the test time was limited and uncertain due to weather and other test projects on the structure at the time of the test, the EMA was limited to two different set-ups. As the tests were beginning, the engines controlling the azimuth and elevation drives were being adjusted. Therefore, the dish was set in safe mode, elevation -70° and azimuth -180° and the first test set-up was performed on this set-up. The other test set-up was performed on elevation 0° and azimuth -180°. These set-ups were chosen in order to have two quite different set-ups and because in both cases there was at least one position chosen by the EFI that allowed a vertical measurement direction where the weight could be dropped from.

During the morning on the first day there were wind speeds between 2.0-6.5 m/s^2 and on the afternoon between 2.4-8.2 m/s^2. The first and second set for the -70° set-up were measured during the morning and the afternoon respectively. The second day was more windy with a mean wind speed at 5.5 m/s^2 but with as much as 12.4 m/s^2 in the gusts, [26]. The last two sets on the -70° set-up and the the two sets on the 0° set-up were measured that day. During the test procedure, the number of accelerometers were chosen as 13 for the -70° set-up and 6 for the 0° set-up.

The load was applied in form of a 10 kg water carrier tied to the structure with a fishing line, see Figure 3.4. To be able to reattach the water carrier more quickly, a hanging device was constructed on the second day of testing, which consisted of a safety hook, and two plates tied together with the fishing line. The first day of testing, the fishing line was tied directly to the water carrier which took longer time. The weight of the mass needed was determined by trial-and-error tests to obtain a response distinguishable from the noise. To apply the load, the fishing line was burned off using a lighter. This method was chosen instead of for example using scissors, in order to avoid external impact and make the test as repeatable as possible.

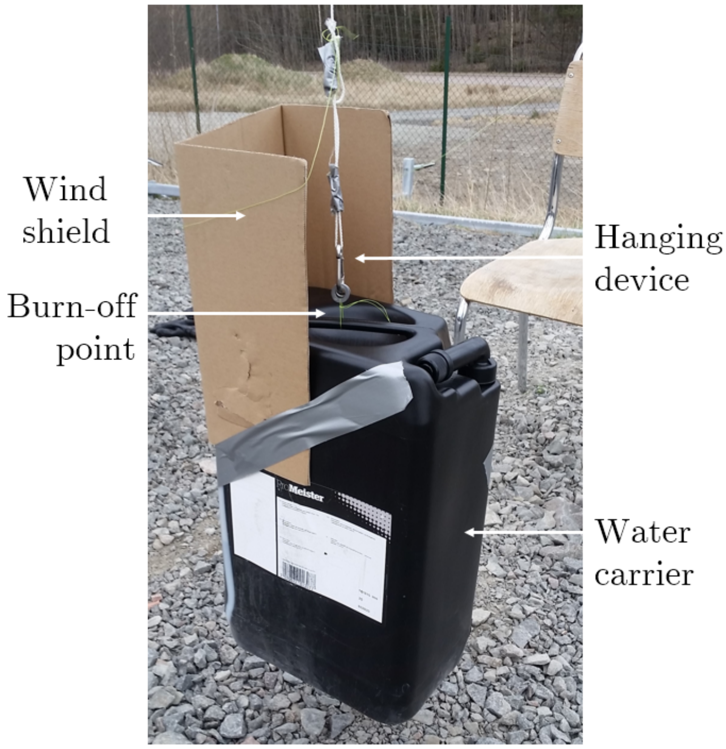

Figure 3.4: The suspension of the weight used in tests.

For each set-up, the test started with the dish being maneuvered to the considered elevation angle and azimuth angle. The accelerometers were mounted onto the structure in the desired measuring direction with beeswax, see the left Figure 3.5. The accelerometers were mounted on four of the determined positions where one was the location where the load would be applied, in the direction of the application. Since the structure is large, an aerial work platform was used to approach the structure. Coaxial BNC cables with an impedance of 75 Ω connected the accelerometers to the signal toolbox and the cables were taped to the structure so that they were hanging loosely, see the right Figure 3.5. This was to avoid pulling the accelerometers, which could affect the results. The signal toolbox was connected to a computer with QuickDAQ installed. The weight was attached to the structure using the hanging device and the oscillation caused by hanging the weight was allowed to die out before the measurements started. When the surroundings were calm, the recording started and the acceleration at each accelerometer was measured with a frequency of 5000 samples per second. The fishing line was burned off without touching the line in order to avoid interference and the recording continued for as long as it took for the oscillations to surely die out and the recording was paused. The weight was once more tied to the structure with the fishing line and the procedure was repeated. Between 15 and 22 drops were performed for the different sets. Initially 15 repetitions were performed, but for the later sets, up to 22 repetitions were done. The updated hanging device enabled quicker hanging of the weight which meant more repetitions could be done. After all drops were done, the three accelerometers not positioned at the weight were moved to new positions and a new test set commenced.

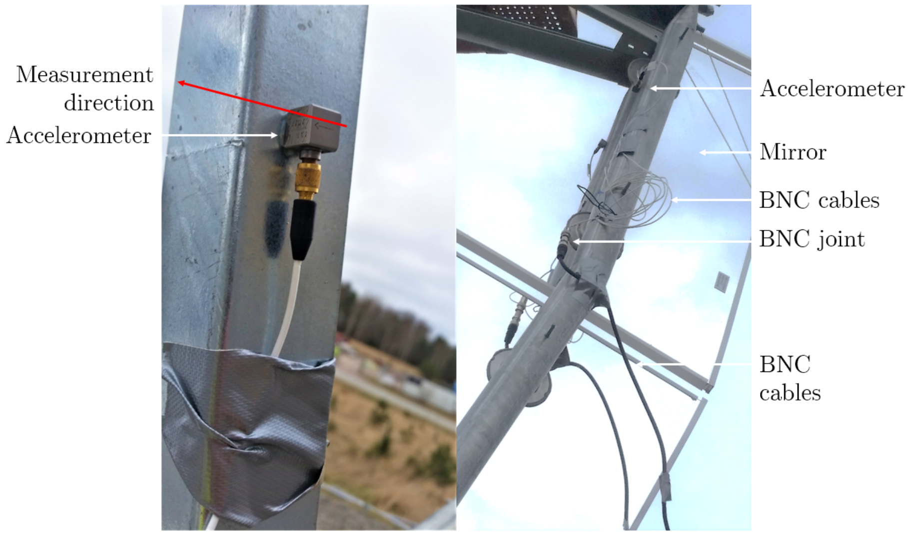

Figure 3.5: The mounting of the accelerometers.

3.2.3 Signal Processing

Signal processing for this project was done in Matlab. Acceleration was measured and recorded during the tests and resulted in raw data. The same test was repeated 15-22 times and hence, the raw data consisted of many blocks, that were similar to each other. The idea is to average all of these blocks in order to obtain one realistic response. Benefits obtained by using this method are that irregularities in the response due to wind will to some extent be cancelled out and that interference in single measurements could be neglected. The first step in the signal processing was to extract all of the short blocks from the original raw data signal. With all blocks separated, aligning was performed, see section 2.2.2.2. When trying to align the signals during a too large time interval, the aligning was unsuccessful. The reason for this is that the correlation between the blocks was highest just after the drop and later on the response was impaired by the wind. Therefore, only about three seconds just after the drop were used for the aligning. This was done for each block and resulted in an offset describing how much each block would have to be delayed in order to fit the previously block. After finding out the offset between the small three seconds blocks, the whole blocks were offset equally and the full blocks were aligned to each other. Now, with the blocks aligned, they were observed in order to distinguish irregularities and differences. Blocks that differ too much from the others or have severe interferences were removed. For example, interferences may have occurred if the structure was touched or the aerial work platform started. For all remaining blocks, linear averaging was performed, see section 2.2.2.3.

This procedure was done for each accelerometer. To create a transfer function, and finally a state space model, an output and input is needed. The response is the output and the loading is the input. The loading was applied in such a way that it correlated with the exact moment when a visible response from the reference accelerometer could be seen. The reference accelerometer was the accelerometer located at the loading point. For all remaining accelerometers, the force was applied at the same time step as it was applied for the reference accelerometer. This aligned them relatively to the reference accelerometer. The same procedure was repeated for all the test sets. Since the start of all test sets was defined by the response of the reference accelerometer when applying the load, all sets became aligned and finally all accelerometers were aligned to each other.

The input and output data was filtered using a Butterworth filter of order 5, to exclude high frequencies associated with noise. As there was a lot of information in the beginning of each block, when the load is applied, but not as much in the end of the blocks, when there is a lot of wind, an exponential window was applied. The filtered and windowed data were used to create the FRFs which were estimated out of the the load and the response for each accelerometer. From all of the FRFs, a state space model was approximated, describing all FRFs.

The state space models were estimated in the Matlab system identification toolbox, using the N4SID algorithm, see section 2.2.2.6. All the estimated transfer functions were imported into the system identification toolbox where a suitable frequency range could be selected. The frequency range was chosen as 0-9.6 Hz, to only focus on the lowest frequencies. As there were a lot of low frequencies, it was difficult to distinguish between the frequencies, and difficult to estimate if a peak in the FRF was indeed an eigenfrequency excited by the tests, or by the wind, or if it was noise.

Finally the order of the model is decided. Half the order is the number of frequencies that is captured by the model. However, it could be seen that not only the larger visible peaks, but also some smaller peaks were captured by the model and hence a suitable model order for this case needed to be higher than the number of larger visible peaks.

The quality of the state space model was determined by a couple of criteria. Firstly, the system identification toolbox calculates a correlation index that determines how close the approximation is to the FRF, where 100 is 100 % correlation and 0 is no correlation. As a rule of thumb, correlation above 90 % can be seen as a good estimation. However, for this complex case, a lower value can be sufficient. Secondly, this can also be done manually by observing the state space model and the FRF at the peaks. If the model correlates well with regards to amplitude and frequency at the peaks, poor correlation in other places can be acceptable.

From the state space model the eigenvalues and eigenvectors could be extracted, see section 2.1. These were then compared to the eigenfrequencies and mode shapes from the FEA for the positions used in the different set-ups.

3.3 Comparing Finite Element and Experiments

The FEA data and the data from the EMA, were compared using the Modal Assurance Criterion, MAC, see Equation (2.31).

Looking at the frequencies, for those from EMA and FEA that were similar, the eigenvectors were studied closer. In order to improve the correlation, where there was a difference in sign between the value in the eigenvector for a certain mode for a certain sensor, the sign was changed across all modes to see the difference in correlation. This was done for several modes to see how changing the sign affected the other modes. The reason for this is that a sensor could have been placed in the wrong direction during tests, and thus the result will be different. To further investigate the impact of each sensor, an eCOMAC analysis was performed, see Equation (2.33).

3.3.1 Calibration

To calibrate the FE model some parameters where changed to achieve a better correlation between the test data and the FE. This was initially supposed to be performed in the Matlab Toolbox FEMcali together with the FE solver Nastran. However, since the analyses were done in Ansys Apdl, the FEMcali app needed to be modified to include using the Ansys solver, or the Ansys model needed to be transferred to Nastran. Both of these methods were evaluated but they were considered too time consuming and outside of the scope of the thesis.

By analysing the results obtained from changing certain parameters from the nominal, original value, calibration was done. This can be seen in Table 3.4.

Table 3.4: Calibration metric.

		Nominal	**Modified**
Full Calibration	$\boldsymbol{E}$	200 GPa	+7% -7% +3% -3%
	$\boldsymbol{\rho}$	7850 kg/m^3	+5% -5%
	$\boldsymbol{\nu}$	0.3	0.28 0.32
Partial Calibration	$\boldsymbol{\rho}$	7850 kg/m^3	+5% -5% +8%
	$\boldsymbol{\nu}$	0.3	0.28 0.32
			$\boldsymbol{E}$ +7% $\boldsymbol{\rho}$ +5%

The Young's modulus, **E** was modified to become seven and three percent higher as well as seven and three percent lower. The Poisson's ratio, $\boldsymbol{\nu}$ was changed to 0.28 and 0.32 and the density, $\boldsymbol{\rho}$ was modified five percent, both higher and lower. In order to more closely study the effect of which parts that were subjected to calibration, it was done in two parts, full and partial calibration, see Figure 3.6. For each calibration, the result was compared to the measured data, in terms of the frequency and the eigenmodes. After the initial calibration, another partial calibration of increasing the density eight percent from the nominal value was done. There was also one cross-calibration done, increasing the Young's modulus seven percent and at the same time increasing the density five percent. There was however no further cross-calibration, that is changing more than one parameter at once compared to the nominal values. In order to save computational time, the analyses for the calibration were only done for frequencies up to 15 Hz.

For each of the changed value, a solution was once more calculated in the FE solver and the eigenvalues and eigenvectors were extracted. The new eigenvectors were compared to the test results with MAC and the result was analysed to see if the correlation had improved or not.

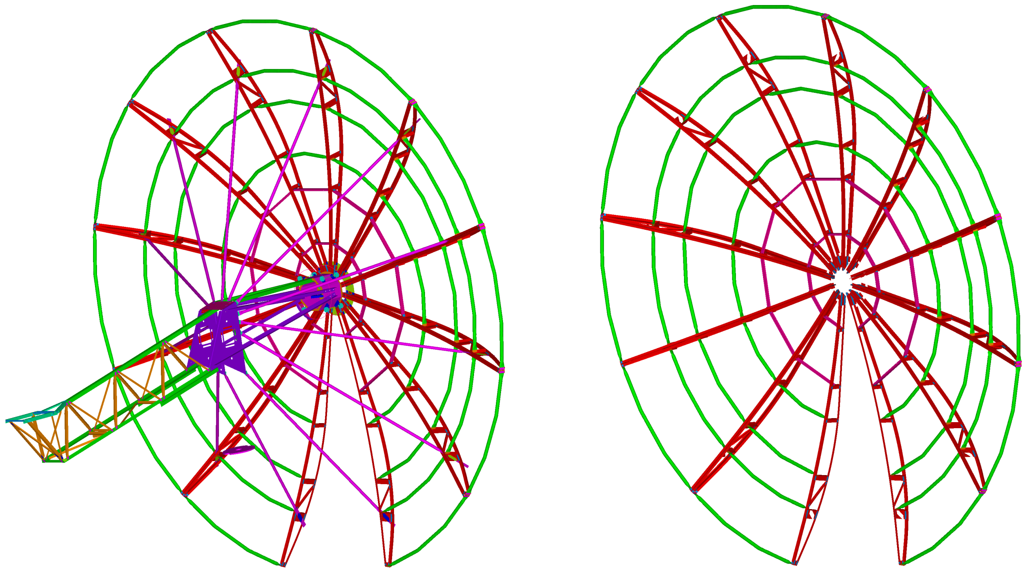

(a) **(b)**

Figure 3.6: Parts used for full calibration, (a) and partial calibration (b).

3.3.2 Validation

The validation of the model consisted of choosing the parameter values which gave the best result from the calibration and using these for the 0° set-up. For this set-up the same signal processing was done as for the −70° set-up. The model using nominal values was compared to a model with calibrated parameters, to see if the same behaviour as for the −70° set-up is shown also for this set-up.

4 Results

The results obtained from using the described methods and theories are presented in this chapter. First, the results from the FEA are presented, followed by results from experiments, including the signal processing and system identification. Lastly the results from the comparison between the experiments and FEA are shown, including before and after calibration and validation.

4.1 Finite Element Analysis

In Table 4.1 the mode shapes for the -70° set-up are described.

Table 4.1: Mode shapes for chosen modes for -70° set-up.

Mode	Frequency [Hz]	Mode shape described
1	0.67	Dish rotating
2	2.02	Left-Right bending
3	2.28	Up-down bending
4	2.56	Boom and dish twisting around elevation drive
5	3.59	Mostly inner part of dish twisting
6	4.63	Boom and Dish rocking back and forth
7	5.60	Boom twisting
8	6.08	Only inner dish twisting
9	7.29	Boom twisting a lot, dish twisting a little
10	7.66	Cross beams at empty sector bending out-of-phase
11	8.37	Cross beams at empty sector bending out-of-phase and boom twisting
12	8.96	Cross beams at empty sector bending out-of-phase, boom twisting, and outer circle beams bending
50	14.43	Boom twisting, umbrella beams bending and outer circle beams bending out-of-phase
67	17.03	Outer circle beams bending in- and out-of-phase
68	17.44	All circle beams bending in- and out-of-phase, boom twisting
75	19.66	All circle beams bending in- and out-of-phase, umbrella beams and beams connecting elevation drive to dish bending

The first four modes for the same set-up are shown in Figure 4.1. The rest of the modes described in Table 4.1 are shown in appendix A. All of these modes can be considered global modes, as there is a lot of movement in the entire structure.

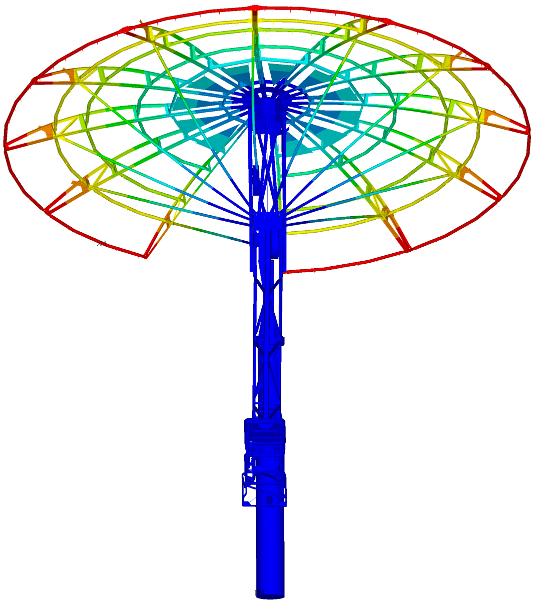

(a) Mode 1

(b) Mode 2

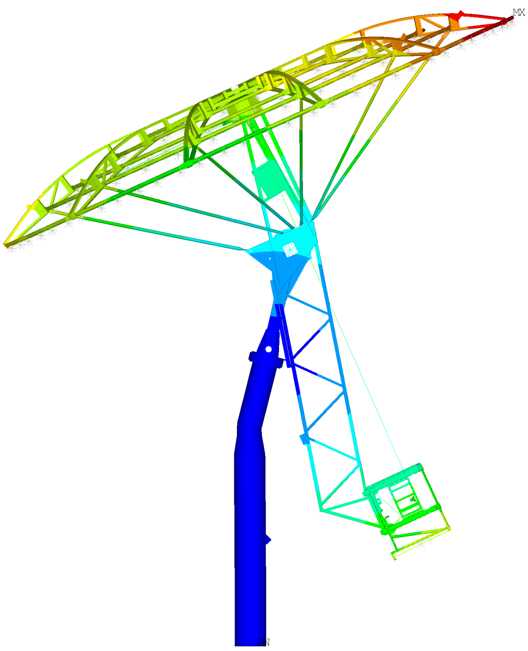

(c) Mode 3

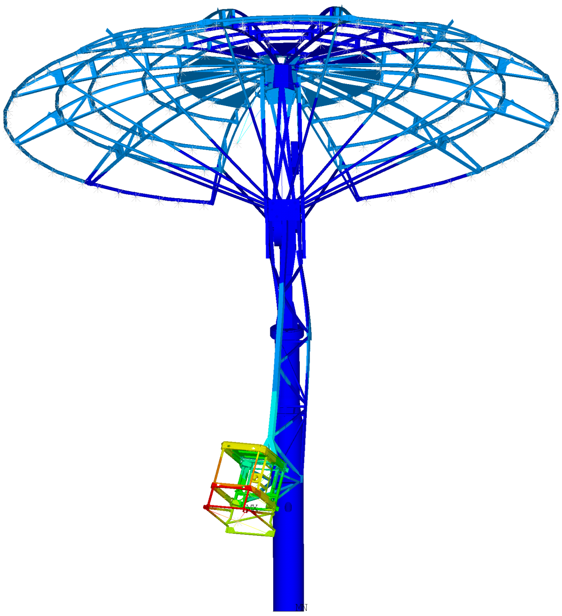

(d) Mode 4

Figure 4.1: First four modes for $-70°$ set-up.

The first four modes for the 0° set-up are shown in Figure 4.2. Comparing these to the modes for the -70° set-up, Figure 4.1, the modes appear to be similar.

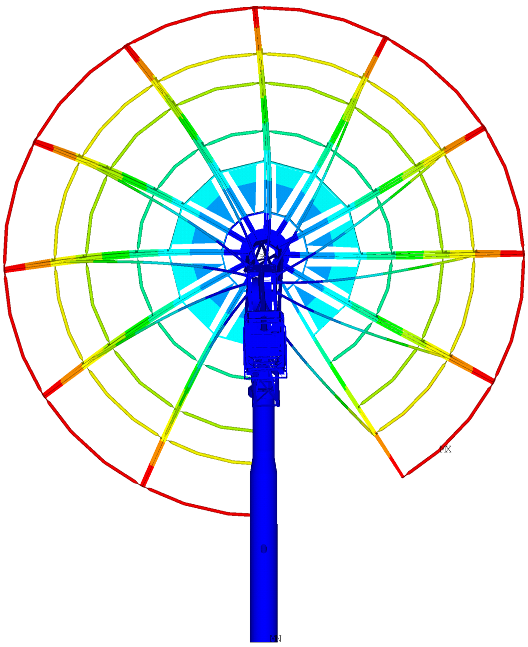

(a) Mode 1

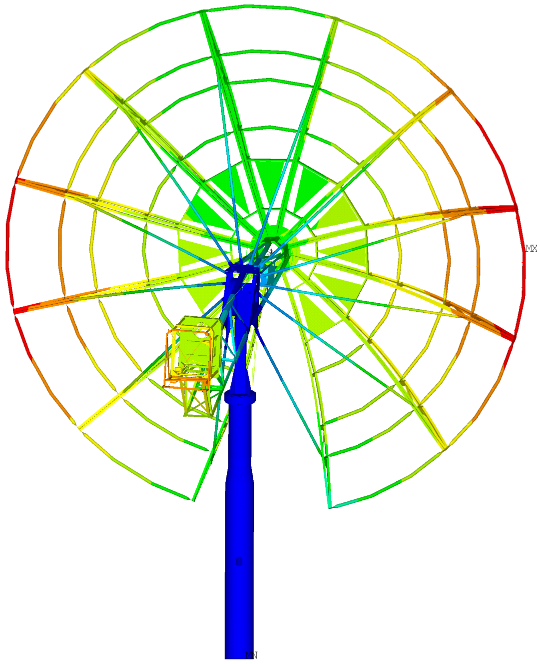

(b) Mode 2

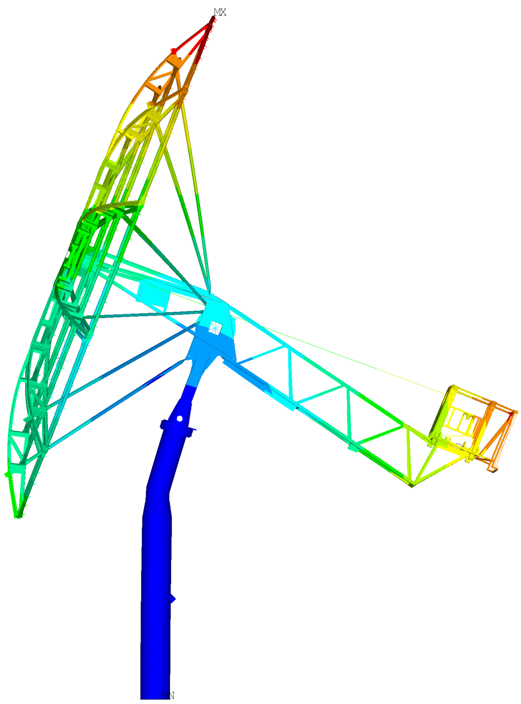

(c) Mode 3

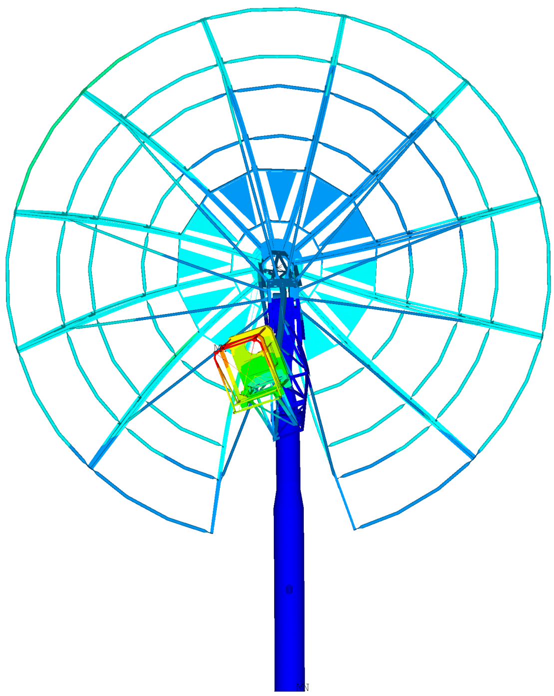

(d) Mode 4

Figure 4.2: First four modes for 0° set-up.

Table 4.2 shows the effective mass and frequencies for the first modes of interest for the -70° set-up. The values in the eigenvectors for these modes for all candidate positions were used as input to the EFI. In the table the largest translational and rotational effective mass over the limit for each mode is highlighted in bold. The limit used for translational effective mass was 148 kg, while the limit for rotational effective mass was 14 800 kgm^2. These limits were set to include the ten most impotent modes. The additional three chosen modes were the lower, fundamental modes. It shows that for most of the lower modes, there appear to be a lot of movement in the structure.

Table 4.2: Effective mass and frequencies for -70° set-up.

	Elevation-70°						
	Freq. [Hz]	Effective mass					
		Translation [kg]			**Rotation** [kgm^2]		
Mode		x	y	z	x	y	z
1	0.67	0.09	0.41	0.00	1507.97	0.72	8886.35
2	2.02	0.89	**472.27**	0.13	**88876.5**	196.74	53151.6
3	2.28	**735.87**	0.018	20.93	2980.45	**89082.5**	75524
4	2.56	7.57	**1108.12**	0.36	54168.7	443.97	**103456**
5	3.59	13.08	109.08	$9.18 \cdot 10^{-9}$	7743.34	525.41	3071.81
6	4.63	**1855.54**	2.25	0.12	214.39	74197.9	**172630**
7	5.60	0.028	**999.49**	0.93	46618.1	85.03	**88604.1**
8	6.08	4.89	19.65	1.12	499.93	612.17	3986.58
11	8.37	90.31	0.07	**305.66**	**30455.1**	13888.2	13888.2
50	14.43	1.39	118.54	1.53	1751.11	320.13	**14868.8**
59	15.74	54.42	3.64	76.95	6244.74	**14886.6**	8729.42
67	17.03	55.74	20.39	108.31	7075.98	**18848.8**	14650.1
68	17.44	16.37	**227.13**	39.80	**16762.1**	6534.78	13237.6
75	19.66	5.62	17.54	29.95	1411.87	1989.85	377.15

A MAC-matrix, see section 3.3, comparing each mode of the unchanged -70° set-up model to all other modes, all calculated from FEA, is illustrated in Figure 4.3a. Figure 4.3b shows the MAC-matrix comparing each mode in the 0° set-up to all the other modes in the same set-up. For both set-ups, the eigenvectors only consist of values that correspond to the measurement points used in tests. Ideally each mode should appear unique, i.e. no other mode should look like it in the measurement points. However, as a limited amount of measurement points are used for tests, modes may appear similar, as significant movement in the mode appear where the are no measurement points.

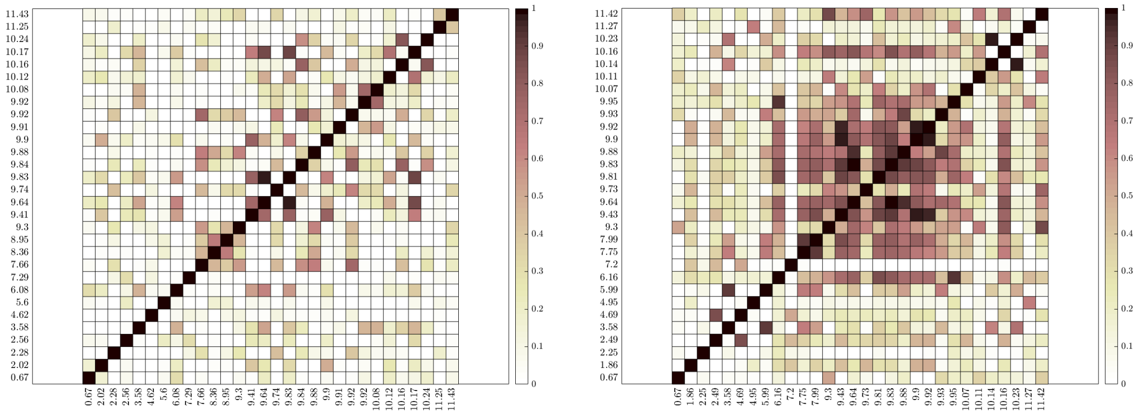

(a) (b)

Figure 4.3: The different modes of the structure compared to each other for (a) the -70° set-up and for (b) the 0° set-up.

All modes have a high correlation to themselves. Some modes also correlate to other modes, such as mode 15 and 17, at 9.64 Hz and 9.83 Hz, respectively, in Figure 4.3a and mode 5 and 8 in Figure 4.3b, at 3.58 Hz and 5.99 Hz.

4.2 Experimental Modal Analysis

Tests were performed in Åmål in April, and are described further in section 3.

4.2.1 Aligning and Averaging of the Signals

The recorded raw signal for all accelerometers in set 2 can be seen in Figure 4.4, where each peak represent a drop, when the weight is released from the structure.

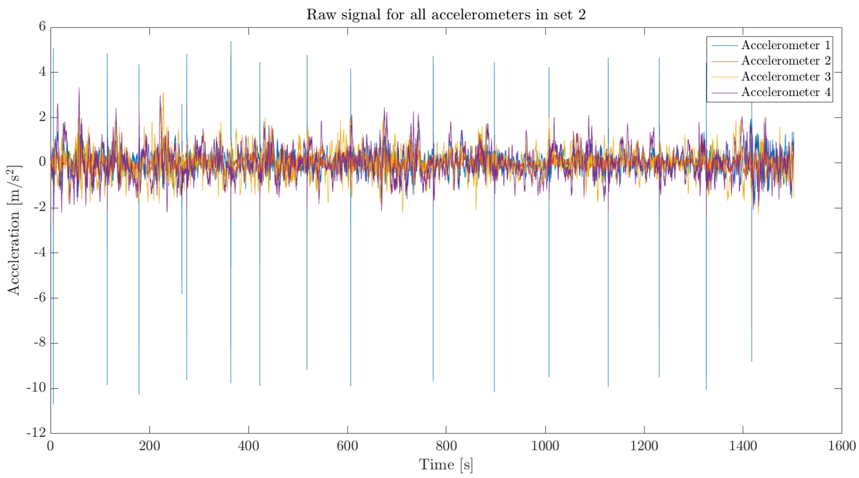

Figure 4.4: The raw data signal for all accelerometers in set 2.

All the aligned blocks from set 1 for accelerometer 1 (the reference accelerometer) can be seen in Figure 4.5 as well as only the kept blocks. The aligned blocks from the other sets and accelerometers can be seen in appendix B. After removing some blocks, the response appears more cohesive, and there is less difference between the blocks.

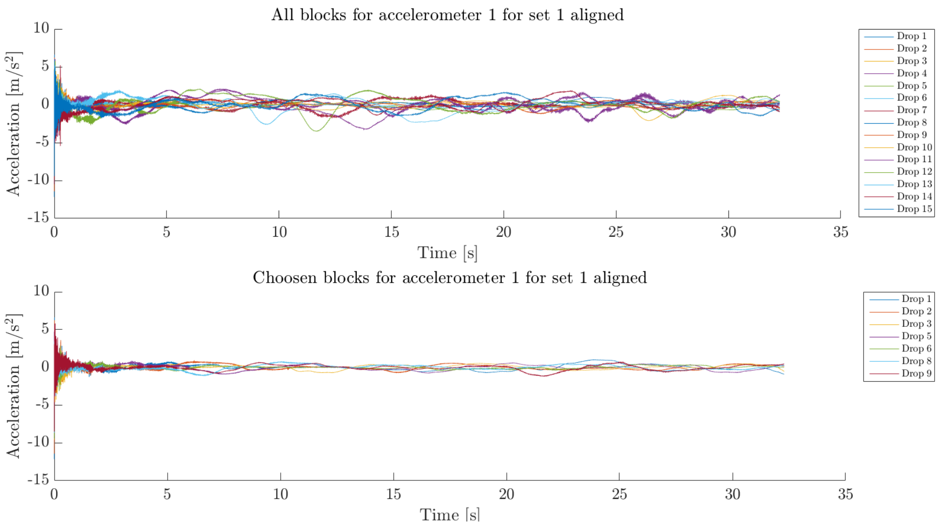

Figure 4.5: All blocks (upper) aligned for accelerometer 1 for set 1 and only the selected blocks aligned (lower).

Enlargements of accelerometer 1 and set 1 at different moments can be seen in Figure 4.6. In the figure, it can be seen that there appears to be a high correlation in phase, but that there is a difference in amplitude. As time passes, the high phase correaltion decreases, as the influence of noise increases.

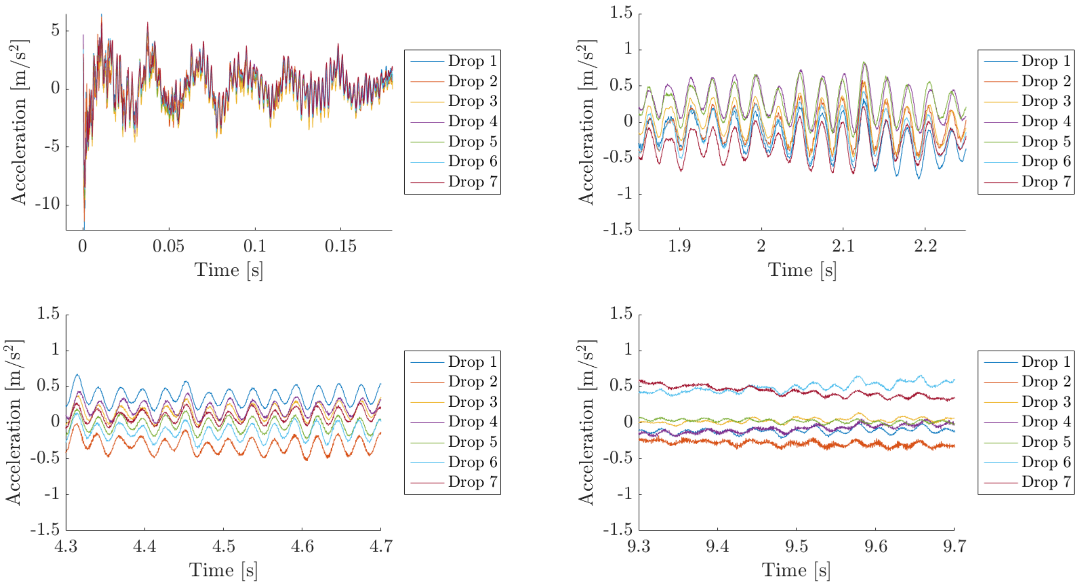

Figure 4.6: Repeatability for accelerometer 1 for set 1 for different blocks.

After the aligning, an average could be calculated in each point of the aligned and selected blocks, resulting in an averaged response. An exponential window is constructed, see Figure 4.7.

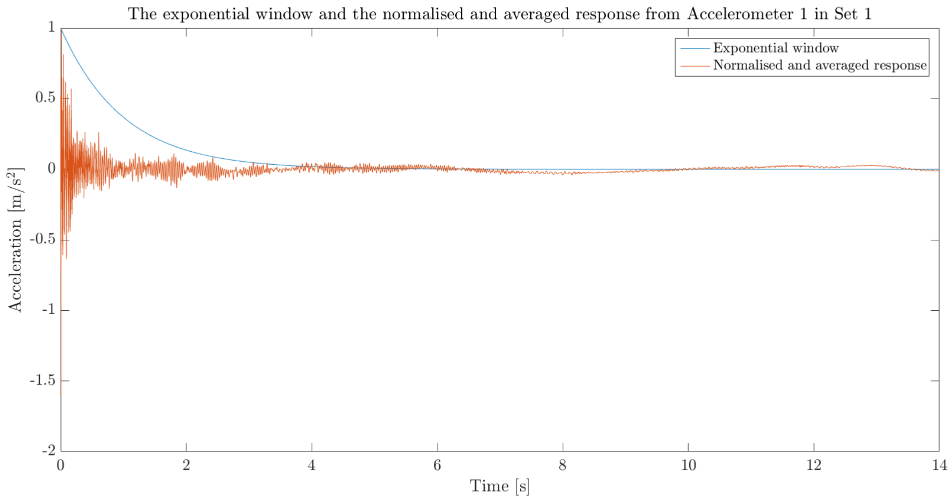

Figure 4.7: The constructed exponential window and the normalised response.

In Figure 4.8 the averaged response for accelerometer 1 and set 1 together with the normalised applied load (upper) can be seen. Before the load is applied, there is noise which has been removed and the exponential window has been applied to the signal (lower). The response a time after the drop, appears to die out more after applying the window. This is the expected behaviour, as the response should only be to applying the load which would die out after a while. As there is still significant response before applying the window after some time, this could be due to wind, and is unwanted.

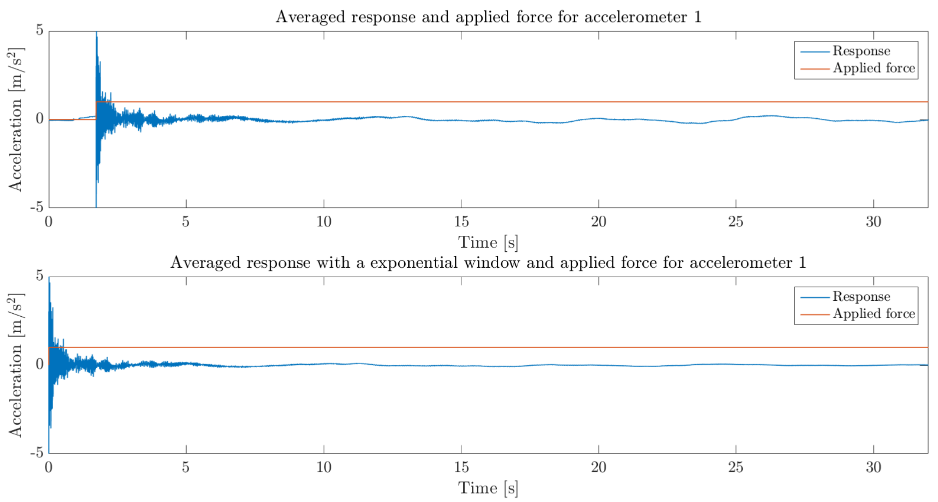

Figure 4.8: Applied force and the averaged response (upper). An exponential window has been applied and signal has been cut where force was applied (lower).

The resulting FRF between the force and the response can be seen in Figure 4.9 for accelerometer 1 in set 1. Each peak should represent an eigenfrequency, however, due to noise, there appears to be more peaks, i.e. eigenfrequencies than was found in the FEA.

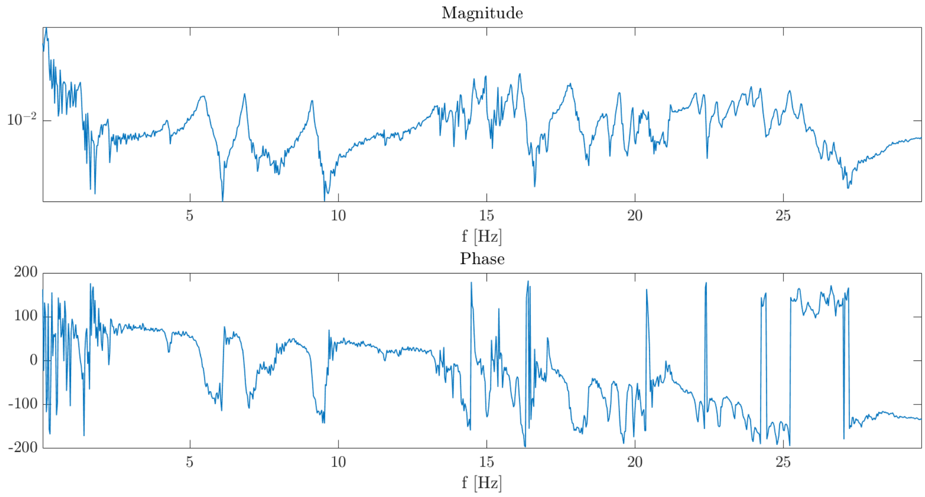

Figure 4.9: Frequency response function for accelerometer 1 in set 1.

The frequency response function for one accelerometer, created after the signal has been averaged and an exponential window has been applied, can be seen in Figure 4.10. In the figure, there fewer peaks, which indicates that some of the peaks were due to noise. The peaks also appear less distinct after applying the window.

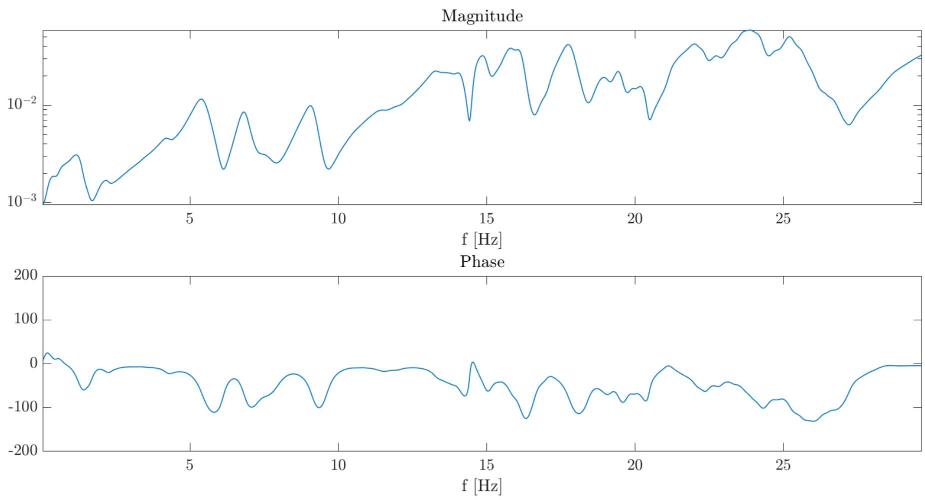

Figure 4.10: Frequency response function of the applied force and the response after an exponential window has been applied.

4.2.2 Creation of a State Space Model

An estimated state space model of order 30 is created and can be seen in Figure 4.11, for two of the accelerometers.

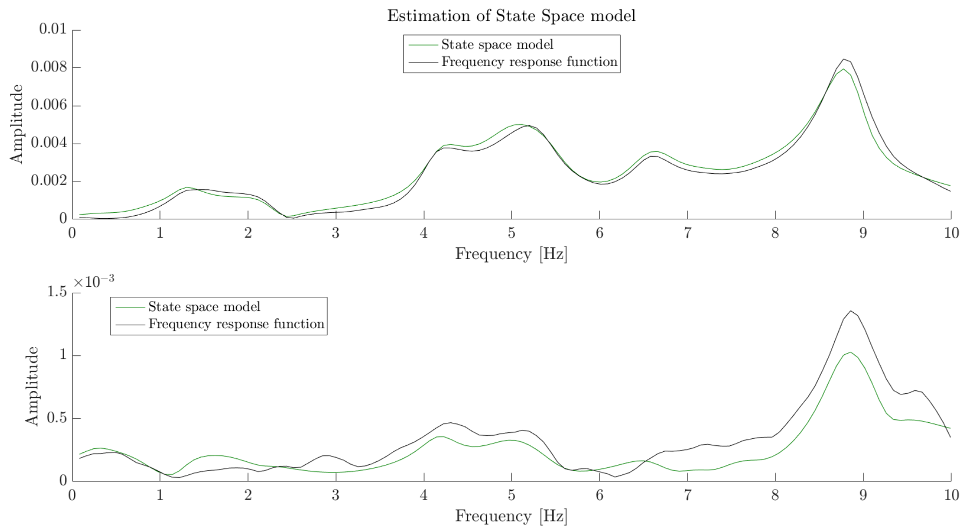

Figure 4.11: Estimation of a state space model with regards to accelerometer 1 in set 2 (upper) and accelerometer 4 in set 1 (lower).

A visual estimation is that the state space model appears to capture the FRF best for accelerometer 1 in set 2, where it has a correlation index of 83 (upper part of Figure 4.11). For accelerometer 4 in set 1, the state space model appears to match the FRF worst and it has a correlation index of 56 (lower part of Figure 4.11).

4.2.3 Test Conditions and Impact of Wind

The first set was measured during better weather conditions than during the other sets. Since one accelerometer was at the same place during all of the measurements, this can be seen when the aligned response for those accelerometers for each set is observed, see Figure 4.12. In the figure, it can be seen that the noise amplitude increases as the wind increases, comparing the upper and lower figures.

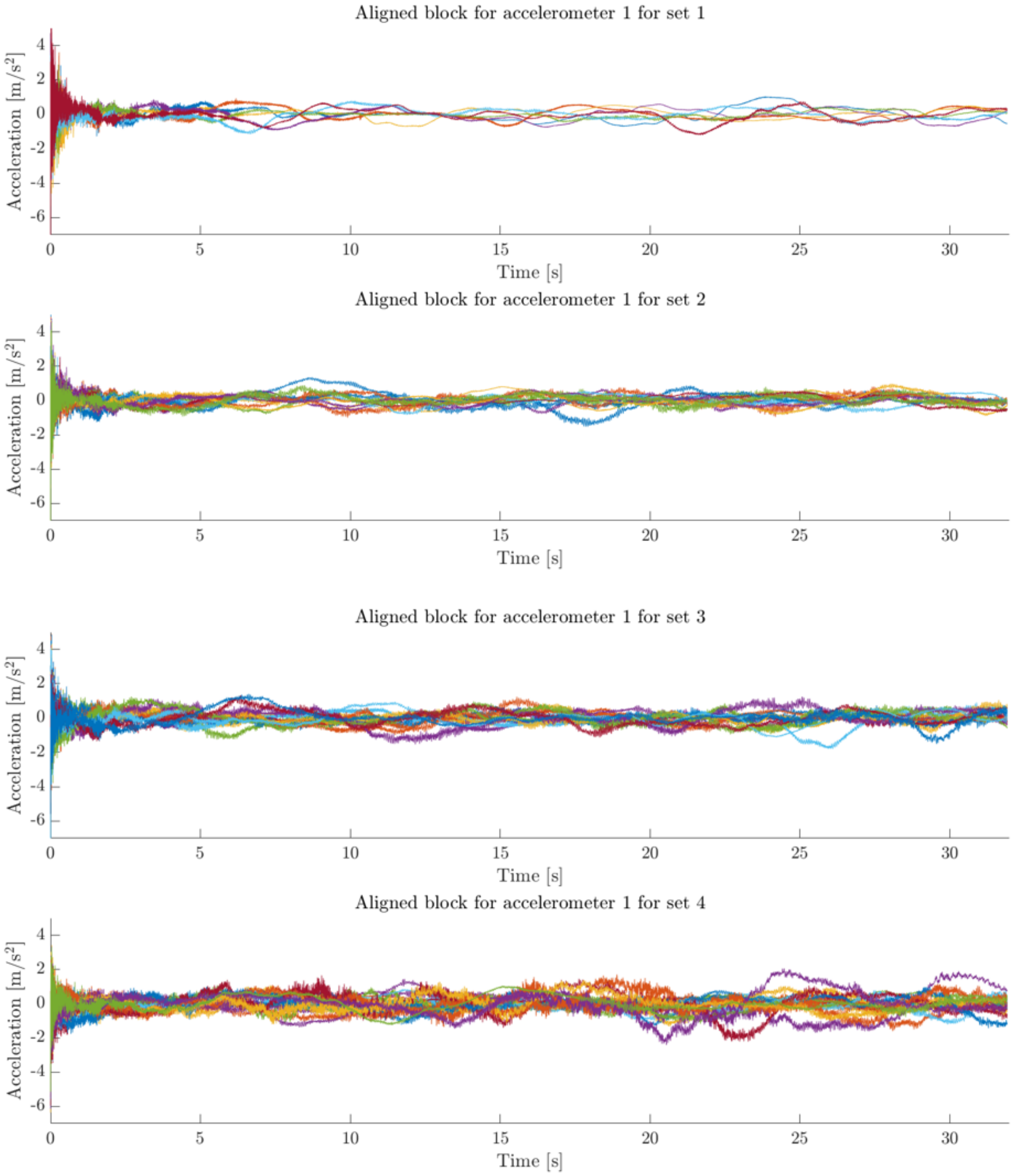

Figure 4.12: Acceleration is plotted against the time for the four sets. In each set, several repeated measurements are plotted in different colors. The influence of the wind can be seen by observing the same measurement but during different weather conditions.

The initial response for the different sets are shown in Figure 4.13, as well as the response 25 seconds after the load has been applied. The response for the different sets appear the most similar just after the drop, but as time passes, the similarities decrease, and the influence of the wind increases.

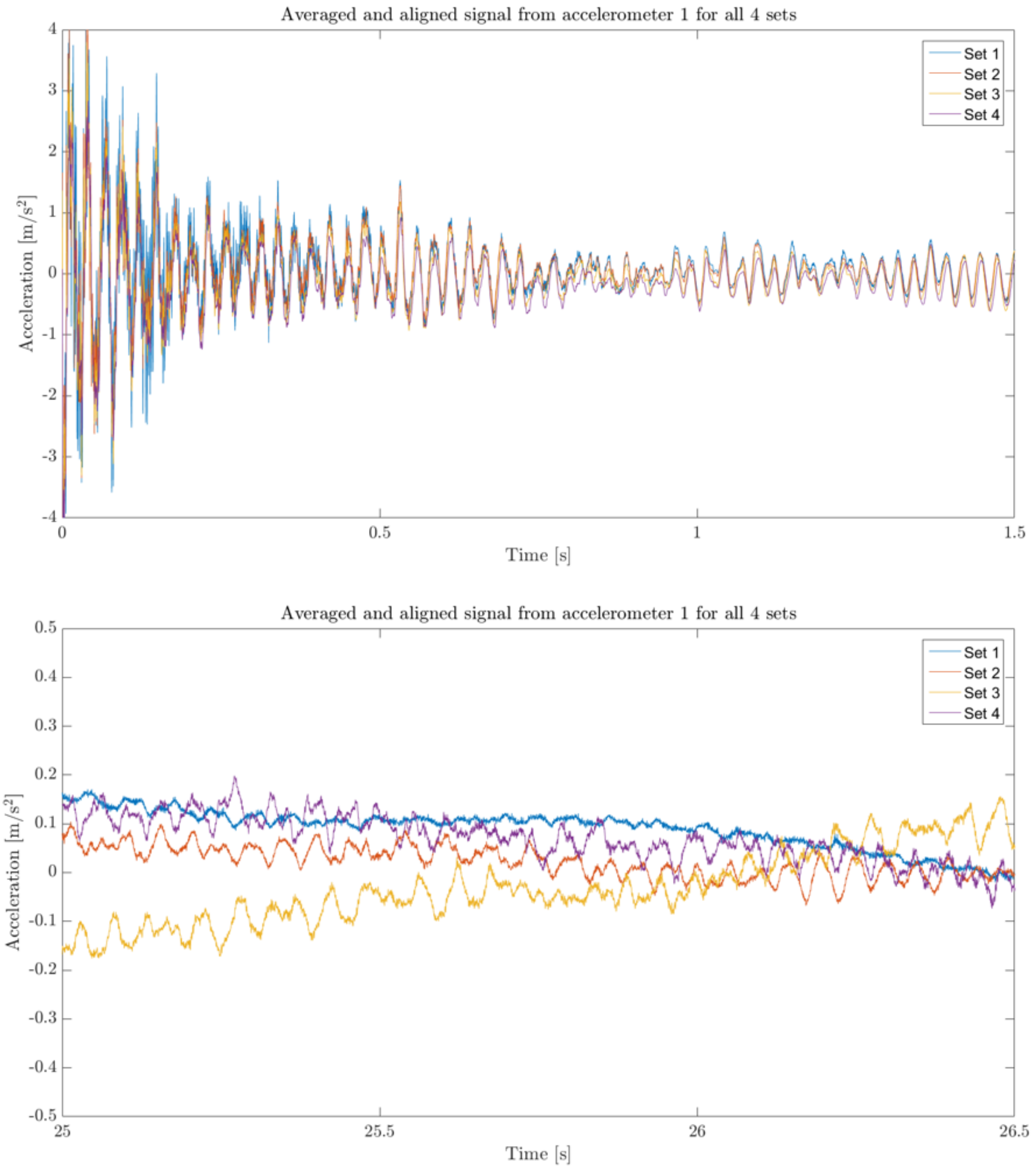

Figure 4.13: The four averaged signals for accelerometer 1 from the four sets are plotted against time and aligned. Enlargements of the beginning (upper) where the load is applied and of 25 seconds later (lower).

4.3 Comparing Finite Element and Experiments

The FEA and EMA are compared before and after calibration.

4.3.1 Calibration

The full and partial calibration of parameters resulted in changes in natural frequencies for the considered modes, see Table 4.3 and 4.4.

Table 4.3: Frequencies, [Hz] before and after calibration for -70° set-up for the full calibration.

		E				**ν**		**Density**	
Mode	**Nominal**	+3%	-3%	+7%	-7%	0.28	0.32	+5%	-5%
2	2.02	1.95	1.93	1.92	1.95	1.94	1.95	1.86	1.97
4	2.56	2.51	2.51	2.47	2.53	2.50	2.55	2.35	2.64
6	4.63	4.61	4.52	4.63	4.57	4.58	4.55	4.50	4.63
7	5.60	5.55	5.49	5.57	5.49	5.51	5.54	5.42	5.65
9	7.29	7.32	7.15	7.43	7.06	7.22	7.24	7.10	7.39
11	8.37	8.46	8.35	8.49	8.24	8.38	8.39	8.32	8.40

Table 4.4: Frequencies, [Hz] before and after calibration for -70° set-up for the partial calibration.

		ν		**Density**			**E +7%**
Mode	**Nominal**	**0.28**	**0.32**	+5%	-5%	+8%	**ρ +5%**
2	2.02	1.91	1.87	1.88	1.98	1.91	1.93
4	2.56	2.45	2.57	2.40	2.46	2.56	2.45
6	4.63	4.54	4.54	4.55	4.55	4.58	4.57
7	5.60	5.50	5.51	5.48	5.55	5.51	5.50
9	7.29	7.22	7.23	7.20	7.25	7.24	7.22
11	8.37	8.34	8.35	8.33	8.38	8.31	8.37

Figure 4.14a shows the MAC-values for the comparison between the FE model and the state space model of order 30. In the MAC-matrix, the correlation between modes 2, 4, 6, 7, and 9 from the the FEA and modes 3, 5, 6, 8, and 9 from the test is high. The MAC-values for these modes are on average 0.737 and the frequencies seem to fit well. A MAC-matrix between the tests and a calibration of the FE model where the Young's modulus density and for the dish, partial calibration, is increased by 7 % and 5% respectively, is shown in Figure 4.14b. The average MAC-value is now 0.74.

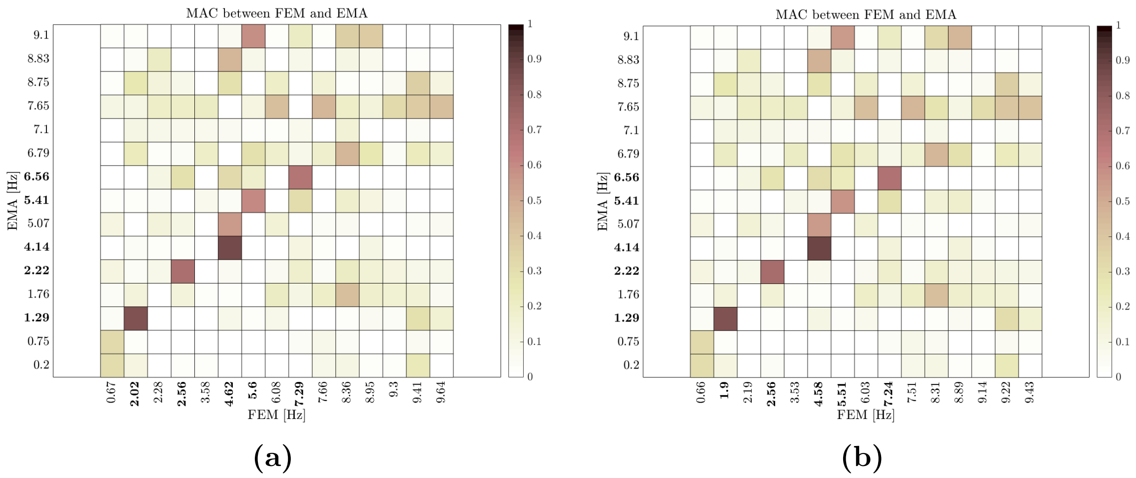

Figure 4.14: Comparison between EMA and FEA with MAC for the -70° set-up for (a) nominal model and (b) calibrated model.

All frequencies and MAC-values for the paired comparisons for the -70° set-up are shown in Table 4.5. All frequencies from FEA appear closer to the EMA, apart from the frequency for mode 4 from FEA which is unchanged. The MAC-value for modes 4, 6, and 9 from FEA are improved, while the MAC-value for mode 2 is unchanged, and for mode 7 the MAC-value has decreased.

Table 4.5: Frequencies and MAC-values for -70° for matching modes before calibration (a) and after (b).

(a)

EMA		**FEA**		
Mode	Freq.	Mode	Freq.	MAC
3	1.29	2	2.02	0.84
5	2.22	4	2.56	0.71
6	4.14	6	4.62	0.86
8	5.41	7	5.60	0.61
9	6.56	9	7.29	0.67

(b)

EMA		**FEA**		
Mode	Freq.	Mode	Freq.	MAC
3	1.29	2	1.90	0.84
5	2.22	4	2.56	0.73
6	4.14	6	4.58	0.89
8	5.41	7	5.51	0.58
9	6.56	9	7.24	0.70

The frequency correlation for that state space model and the calibrated FE model is shown in Figure 4.15

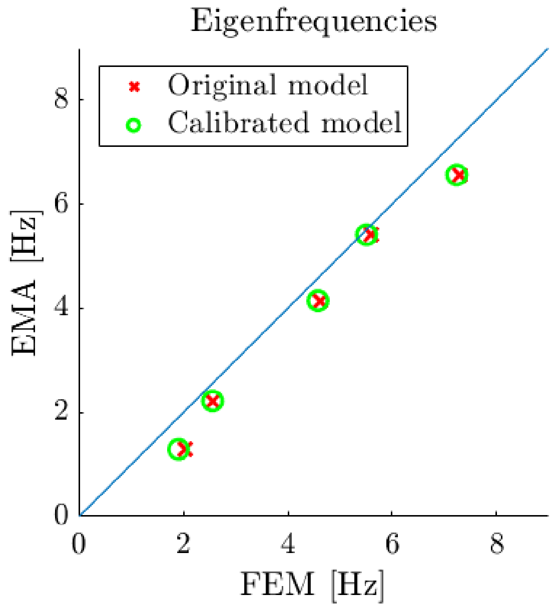

Figure 4.15: Frequency correlation between EMA and calibrated FEA.

4.3.2 Validation

The MAC-values for the comparison between the FE model and the state space model of order 28 is shown in Figure 4.16a. The correlation between mode 1, 3 and 5 from the the FEA and mode 1, 3 and 6 from the test are recognized. The average MAC-values for these modes is 0.797 and the frequencies are similar. After doing the same calibration that was done for the -70° set-up to the 0° set-up, a MAC-matrix was created, see Figure 4.16b. The average MAC-value is now 0.804.

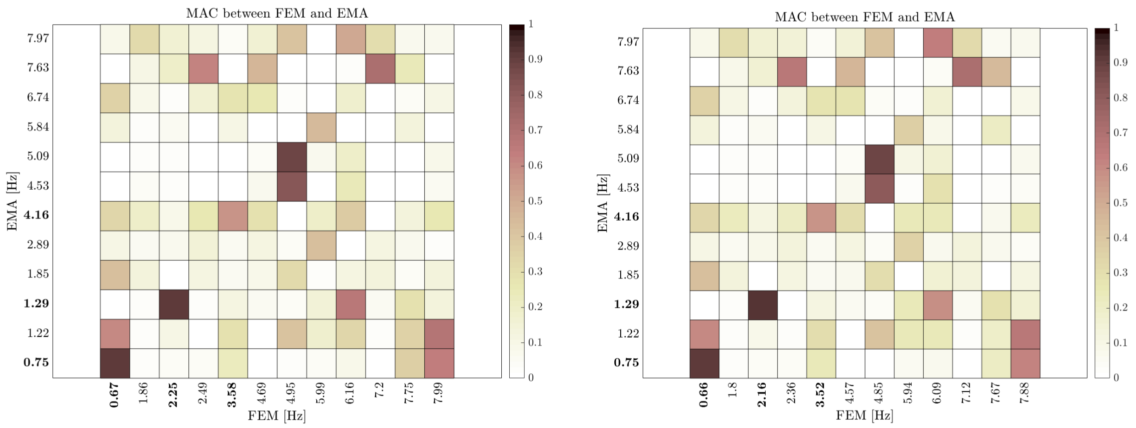

(a) (b)

Figure 4.16: Comparison between EMA and FEA with MAC for the 0° set-up for (a) nominal model and (b) calibrated model.

All frequencies and MAC-values for the paired comparisons for the 0° set-up are shown in Table 4.6.

Table 4.6: Frequencies and MAC-values for 0° for matching modes before calibration (a) and after (b).

(a)

EMA		**FEA**		
Mode	Freq.	Mode	Freq.	MAC
1	0.75	1	0.67	0.91
3	1.29	3	2.25	0.91
6	4.16	5	3.58	0.56

(b)

EMA		**FEA**		
Mode	Freq.	Mode	Freq.	MAC
1	0.75	1	0.66	0.92
3	1.29	3	2.16	0.93
6	4.16	5	3.52	0.57

Figure 4.17 shows the nominal frequency correlation for the 0° set-up. The correlation for the calibrated values that gave the best correlation for the other set-up, increasing the Young's modulus 7 % and the density 5% are also shown in Figure 4.17.

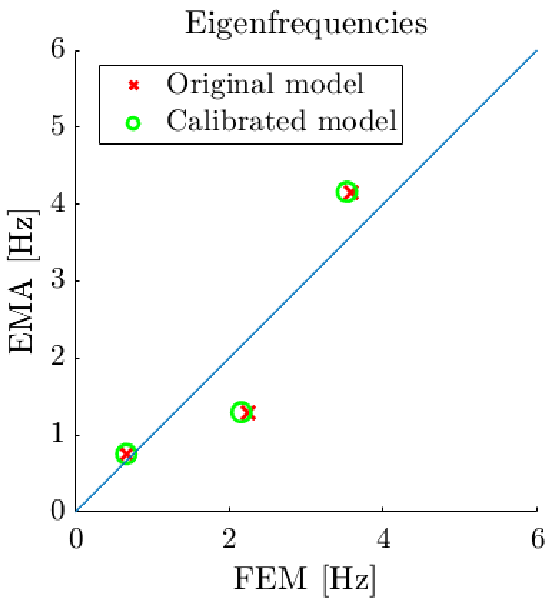

Figure 4.17: Frequency correlation for the 0° set-up for nominal model and the calibrated model.

The quality of each accelerometer was analysed with eCOMAC, see Figure 4.18 and Figure 4.19. The analysis is done for both the current state space model and for an alternative, in order to see if the trend is the same. For the -70° set-up accelerometer 3 and 4 in set 3 were the poorest and for the 0° set-up were accelerometer 1 in set 1-2 and accelerometer 3 in set 2 poorest.

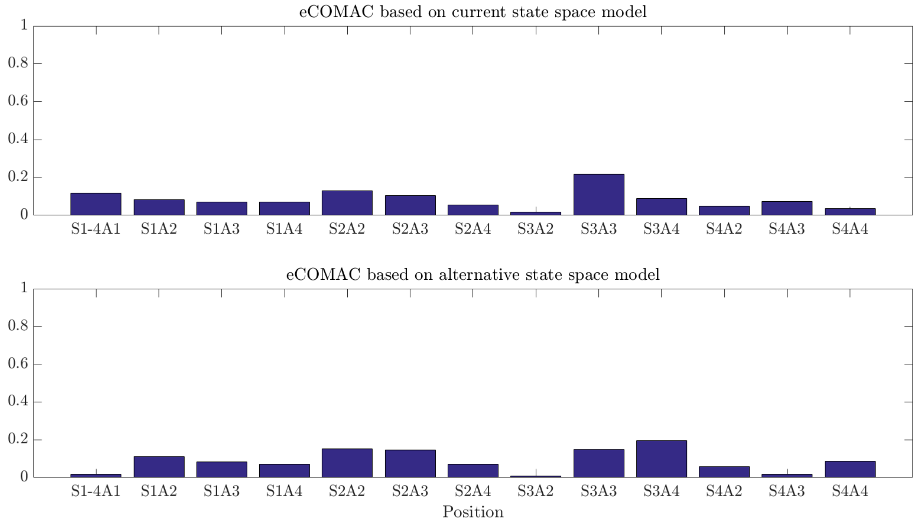

Figure 4.18: The result from each accelerometer is analysed with eCOMAC for -70° set-up. Low values indicate a good response from that accelerometer.

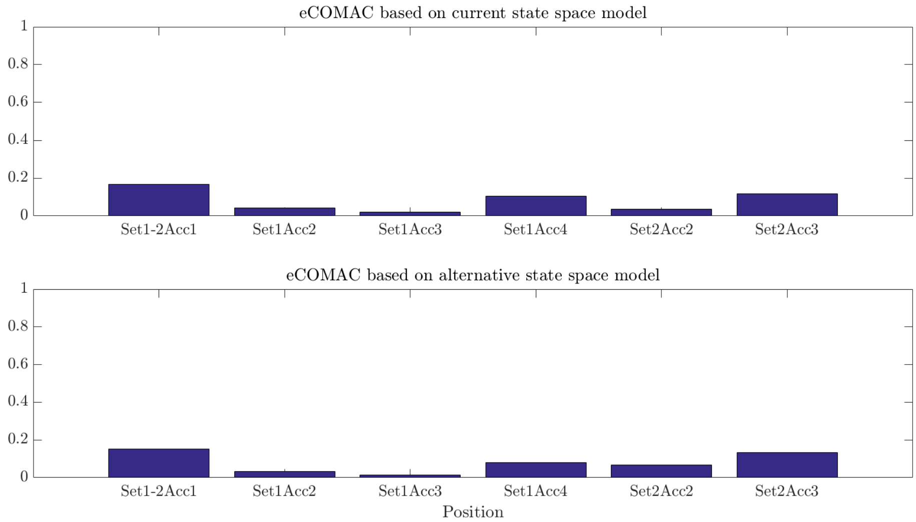

Figure 4.19: eCOMAC-values for each accelerometer for 0° set-up.

5 Discussion

This section discusses the results in the previous section, as well as some of the methods used. Both FEA and EMA as well as comparison between these are discussed.

5.1 Finite Element Analysis

When comparing the modes calculated in FEA for the -70° set-up and the 0° set-up to themselves, the distinctiveness of most modes can be demonstrated, see Figure 4.3a and Figure 4.3b. However, a few modes correlate to other modes as well such as mode 15 and 17 in the -70° set-up, see Figure 4.3a. It is important to note that the figure only shows the comparison between the eigenvectors in the points used for the tests. Hence, the high correlation to several modes could be due to the accelerometer positions, where possibly little movement was detected in both mode 15 and 17, at 9.64 Hz and 9.83 Hz respectively, and thus they will appear the same. But since the accelerometer positions were chosen in order to capture the lower modes, this is to be expected. Consequently, the lower modes are significantly more distinct, which can be seen clearly in Figure 4.3b for modes below 7.2 Hz. This further indicates that the lower modes are good to focus on, since the risk of mixing up modes when comparing them to results from EMA is lower.

The impact of using more measuring points is also illustrated in Figure 4.3a and Figure 4.3b. There is much more cross-correlation in Figure 4.3b than in Figure 4.3a which is probably because only six measuring points were used, instead of 13 for the -70° set-up. Figure 4.3a also contains false correlation, but to a lower extent. More measuring points would probably counteract this problem further.

5.2 Experimental Modal Analysis

There are several aspects of the EMA which are discussed in this section.

5.2.1 Placement of Accelerometers

When performing the EFI to determine sensor placement, the chosen interesting modes were mainly determined by looking at the largest effective mass. With those modes, accelerometer positions were calculated with EFI. Finally, one of those accelerometer positions was chosen as an excitation position. However, when exciting the structure at this position, not all the modes that had been considered interesting were excited. Thus, a better way to perform this procedure would have been to iterate all the steps once more; when the excitation position was chosen, determine which modes that would be excited and use these modes in the EFI for calculating the candidate positions. In this way, the model could be validated for these modes as well.

5.2.2 Wind Impact

The impact of the wind has a great effect on the response of the structure. Figure 4.12 shows that the first accelerometer set is clearly exposed to less noise than the following sets. The noise caused by the wind makes the response blurred and less harmonic, which is clearly seen for the later sets. These sets were performed on the second day of testing, when there was considerably more wind. However, looking at Figure 4.13 the response due to the applied load, can be seen clearly at the start of the signal. Even though the signals look quite different, the repeatability is initially very good. Just after the load in the -70° set-up is applied, the signals are well aligned, which can be seen in the upper plot. However, after some time has passed, the aligning is impaired and noise takes over more and more, see the lower plot. In this plot it can also be observed that the three measurements which were exposed to more wind (Set 2-Set 4) have a larger noise amplitude compared to the first measurement, shown in blue.

To perform the measurements during less windy conditions would have been preferable. Still, the wind will always impact in some way when doing experiments outdoors and to account for that, linear averaging was used. By repeating the test several times the wind would be averaged away, since it is irregular. However, since the wind was very strong and mainly in the same direction, it probably did not succeed in removing the effect from the wind completely. Another issue is that the wind was so strong that it could have changed the response that was caused from the snap-back test, as it might have meant that the structure was excited not only vertically, but that there might be a horizontal component as well due to the wind. In that case, linear averaging would not help.

5.2.3 Signal processing

The raw signal from set 2 is shown in Figure 4.4 where all drops are shown consecutively as one signal. It can clearly be seen when the drop occurs, at least for accelerometer 1. The drop causes a response with an amplitude of about 10 m/s^2 and the average noise is at about 1 m/s^2. Hence, the drop creates a response ten times greater than the noise, which is desired to distinguish the response.

The amplitude after the drop differs quite much from one accelerometer to another. For example is Figure B.12 quite high in amplitude. This could depend on temporary gusts. It could also depend on the measuring direction and if that direction naturally is easy moved or not.

When deciding to do several test blocks, the purpose was to have a chance to eliminate failed or poor blocks. In Figure 4.5 the improvement of doing this is striking. Yet, for the blocks in between good and poor, it is difficult to know which should be kept and which should be removed. This was primarily done by studying each set closely to see irregularities. Especially the beginning of the signals was studied, because if the start of the signal was poor, the chance that the rest of the signal also was poor seemed to be greater. However, this method was time consuming and the accuracy of this part could obvious be improved by doing this more thoroughly.

There were difficulties in determining the length used for the signal, in terms of seconds. A too short signal would not capture the harmonic response from the snap-back test, but a too long signal would mean that the influence of the wind, and thereby the differences in the signal would be too great. The decrease in correlation as time passes is shown in Figure 4.6. This could also cause a problem with leakage as a periodic signal is required for the FFT to work accurately. With the use of windows, the length of the signal was less of a problem as the effect is damped at the end of the block, but for tests less affected by wind, it might be a bigger problem. Another issue with choosing the lenght of the signal concerned the lowest frequency modes. As the lowest frequency was around 0.65 for both set-ups, it was important to choose the signal length so that this frequency occurred enough times in the signal. In the end, around 14 seconds of data was used for the FRF, which meant that the lowest frequency was repeated at least 20 times, which was considered enough.

5.2.3.1 Filters and Windows

In the case of this thesis, only the lower frequencies were of interest, as the focus is the fundamental modes. Therefore, there is not the same need to use Butterworth filters on the data to damp higher frequencies, as the frequency range can simply be adjusted to only include the lowest frequencies, in this case, below 10 Hz. The use of an exponential window also means that there is less need for a filter, as the higher frequencies are damped by the window. An exponential window was considered the most appropriate to use, since the most important part of the signal was in the beginning. The slope of the window was determined by trial-and-error test and the constructed state space models for different results were compared and evaluated, resulting in the window in Figure 4.7. The window is applied to the signal in Figure 4.8 where the effect can be seen especially in the end, as the response is damped. In the same figure the applied force can be seen. The force is applied in the exact moment when the response starts. This is important in order to estimate a good transfer function. It could be seen that the quality of transfer function decreased significantly if the load was not applied at the right point.

5.2.3.2 Frequency Response Functions

The FRF in Figure 4.9 is not particularly smooth and contains lots of smaller peaks. These peaks are probably a result mainly of external noise during the measurements and should not be mistaken for eigenfrequencies. This makes it difficult to construct a state space model, since the estimation will try to catch many of these smaller peaks. By applying an exponential window, see Figure 4.8 and Figure 4.10, some of this noise is cancelled out, resulting in a smoother FRF. It is important though, to not cancel out too much of the signal because this could mean that important data is lost and that the estimation instead captures too few peaks and misses eigenfrequencies. A trial-and-error method was used to find an optimal shape of the window that canceled out the right amount of noise.

5.2.4 System Identification

The created state space model is not a perfect copy, but rather a mathematical estimation of the frequency response function. In Figure 4.11 the estimation of the state space model for one better and one poorer output channel can be seen. Even though the correlation index is not as good for both outputs, the overall correlation can be considered adequate. This is because when observing the estimations in the picture, the peaks seem to be located at least at the same frequencies and the amplitude does not differ too much. A better approximation could be found by trial-and-error, if more time would be spent on this, by changing for example the used blocks, the shape of the applied window, the considered frequency range, the order of the state space and the length of the signal. New vibration measurements during calmer weather conditions could probably make it easier to obtain a better fit as well.

It can be seen in Figure 4.11 that the state space model does appear to match the FRF on modes from 4-6 Hz for at least some accelerometers. However, when comparing it to the FEA using MAC, the correlation is not great for some modes, Figure 4.14a. This can be due to the noise from the wind or that the exact spot that the accelerometers were mounted on does not exactly match the element taken in the FEA.

5.2.5 Test methodology

By performing the pre-test on the composite wind turbine blade, the method used in tests could be tried out. The wind turbine blade was part of a substructuring project, and on the blade, FEA had already been done. From the pre-test eigenfrequencies and eigenvectors could be extracted that matched those from the FEA done in the substructuring project. By using the pre-test methodology in the tests on the Dish-Stirling system, the plausability of the results was considered to be good.

5.3 Comparing EMA and FEA

The MAC-matrix that compares EMA and FEA, see Figure 4.14a, does not consist of a diagonal row with black boxes, like for example Figure 4.3a, but shows a distinct tendency towards a strong correlation between modes. When looking at which modes that should have been excited with regards to where the load was applied, see Table 3.3, and where the accelerometers were positioned, see Figure 3.3, the modes 2, 4, 6, 7, and 9 should be detected. If observing Figure 4.14a, these are also the modes that are detected.

5.3.1 Calibration

Looking at how the eigenfrequencies changes for the calibration, both from the full and partial calibration, it can be seen that the result is not always intuitive, see Table 4.3 and Table 4.4. For example for the fourth eigenfrequency, an increased stiffness yielded a lower eigenfrequency than for a decreased stiffness, which is counter-intuitive. This can be due to the complex structure, and it makes the calibration process more difficult. If all frequencies from the EMA were lower than those from FEA, increasing the stiffness could be an intuitive solution. The tables do show however, that this might not be the best approach. Instead, using calibration software, which can cross-calibrate several parameters at once, may be a better approach.

However, when looking at the calibration regarding both increase of Young's modulus and density of the dish, the FE model has improved, see Figure 4.14b. All frequencies have become lower and are closer to the frequencies obtained from the test. The correlation of the eigenvectors has also improved after the calibration which can be seen when comparing the MAC-matrix to the nominal one, see Figure 4.14a.

The calibration in this thesis was only done by changing parameter values. Another point for the calibration can be the modelling of joints between components, and also the boundary conditions. In the FEAs the boundary condition was set as fixed for the degrees of freedom at the bottom of the pillar. However, the real boundary condition might be more like a stiff spring which can allow the pillar to move slightly. Modifying the boundary conditions to more mimic reality can yield a better correlation between the FE model and the tests.

5.3.2 Validation

The validation was done on the 0° set-up. This test was performed with measurements from only 6 different accelerometers. With such few positions that were measured, the position for these were chosen in order to at least capture the first three modes. Looking at Figure 4.16a it can be seen that the capturing of mode 1 and mode 3 was successful (mode two was not excited in this set-up). Also mode 5 is considered to have been captured. Looking at Figure 4.16a there appears to be a high correlation for the 7th FE mode. However, this mode was not excited in tests, and the high MAC-value could be due to the fact that in that mode, there is little movement overall in the chosen accelerometer positions. Altogether the validation of the model is evaluated from result from these three modes and should be seen as an indication if the calibration seems to be right, rather than a fact.

Looking at the results from the eCOMAC, see Figure 4.18 and Figure 4.19, it can be seen which sensors that were the poorest. This indicates that these sensors contribute most to the fact that there was not a perfect correlation between the FEA and EMA. This could be due to measurement faults, or the fact that these accelerometers had the largest response, and thus they contribute more than other accelerometers which all have a fairly low response.

Another issue with using different set-ups for the tests, is that the model cannot be said to be validated for certain modes. Instead it can be said to have been calibrated for the calibrated modes for the -70° set-up, and somewhat validated for the validation modes for the 0° set-up. To further validate the model is very complicated as there are so many set-ups that are used during the operation of the Dish-Stirling system.

6 Conclusions

The problem statement of the project was to perform EMA of a parabolic Dish-Stirling system for Cleanergy. Results from the EMA were to be used to calibrate and validate the FE model. As can be seen in the result the calibration did improve the correlation between the FE model and tests. This means that a calibration has been done that improved the correlation. However, the model cannot be said to be completely validated for the modes in question, as better parameter values that improves correlation potentially can be found through a more extensive testing and calibration metric. The complexity of the structure also poses difficult problems. Since the model would need to be validated for all modes that are of interest, a better calibration and validation set could be used. If more data points are used some data points could be used for calibration and others for validation. On the other hand, fewer tests could have been done.

This thesis exemplifies many of the problems that occur when testing, especially on large complex structures located outdoors. In the discussion chapter many of these problems are highlighted and some solutions are presented.

6.1 Future Work

In order to get better results there are several points that can be included in future work. The main point is to redo tests when there is less wind, to be able to decrease the impact from wind, and make sure that the structure is mainly excited by the snap-back test. However, there are test methods which are based on only subjecting a test object to random noise, and identifying a system with an unknown input. This was beyond the scope of the thesis, but could be a good method for this type of structure. To be able to have a fully validated model, more samples of the structure would be needed for testing, to analyse the spread between samples that are nominally the same. It would also be good if more measurement points were used to be able to capture the response of more of the structure, and to differentiate the modes more from each other, in terms of the eigenvectors.

Another point for future work is to continue to work on the calibration. Instead of changing a few parameters at a time, this could more efficient be done using software such as the Matlab application FEMcali.

A part of the project included preparing tests for performing a similar analysis that was done on the entire structure, on the boom and the engine separately. This could be done to ensure that these components have validated FE models, and then investigate the attachment points and joints to the entire structure. An advantage with this is that these parts can be tested in more controlled environments, e.g. by suspending them indoors, and thereby removing the impact of the wind.

References

[1] Cleanergy. *CSP Systems for solar parks*. 2017. URL: http://cleanergy.com/solutions/#csp-systems (visited on 23/01/2017).

[2] Cleanergy. *Technology*. 2017. URL: http://cleanergy.com/technology/#why-stirling- (visited on 23/01/2017).

[3] U.S. Energy Information Administration. *EIA projects 48% increase in world energy consumption by 2040*. 2017. URL: http://www.eia.gov/todayinenergy/detail.php?id=26212# (visited on 26/01/2017).

[4] Abrahamsson T. *Calibration and Validation of Structural Dynamics Models*. Chalmers University of Technology, Applied Mechanics, 2012-01.

[5] Vibration Data Irvine T. *Effective modal mass and participation factors*. 2015. URL: http://www.vibrationdata.com/tutorials2/ModalMass.pdf (visited on 15/05/2017).

[6] Craig Jr R. R. and Kurdila A. J. *Fundamentals of structural dynamics*. Hoboken, New Jersey: John Wiley & Sons, Inc., 2006.

[7] Avitabile P. 'Experimental modal analysis'. In: *Journal of Sound and Vibration* 35.1 (2001).

[8] Torben R. Llcht Mark Senldge. *Piezoelectric Accelerometers and Vibration Preamplifier*. 1987. URL: https://www.bksv.com/media/doc/bb0694.pdf (visited on 30/05/2017).

[9] Brüel and Kjær. *Measuring vibrations*. 2850 Naerum, Denmark: Brüel and Kjær, 1982.

[10] Cables On Demand. *What is the Difference Between 50 Ohm and 75 Ohm Coaxial Cable*. 2014. URL: http://cablesondemandblog.com/wordpress1/2014/03/06/whats-the-difference-between-50-ohm-and-75-ohm-coaxial-cable/ (visited on 17/03/2017).

[11] Moya A. and Ho C. K. 'Modeling and Validation of Heliostat Deformation due to Static Loading'. In: *ASME 2011 5th International Conference on Energy Sustainability* January 2011 (2011), pp. 547–555.

[12] Kammer D. C. 'Sensor Placement for On-Orbit Modal Identification and Correlation of Large Space Structures'. In: *Journal of Guidance, Control, and Dynamics* 14.2 (1991), pp. 251–259.

[13] Grinstead C. M. and Snell J. L. *Introduction to Probability*. American Matematical society. URL: http://www.dartmouth.edu/~chance/teaching_aids/books_articles/probability_book/Chapter6.pdf (visited on 15/05/2017).

[14] Friswell M. I. and Castro-Triguero R. 'Clustering of Sensor Locations Using the Effective Independence Method'. In: *AIAA Journal* 53.5 (2015), pp. 1–3.

[15] Hemez F. M. and Farhat C. 'An Energy Based Optimum Sensor Placement Criterion and Its Application to Structural Damage Detection'. In: *XII International Modal Analysis Conference (IMAC)* Society of Experimental Mechanics, Bethel, CT, (1994), pp. 1568–1575.

[16] Heo G., Wang M. L. and Satpathi D. 'Optimal Transducer Placement for Health Monitoring of Long Span Bridge'. In: *Soil Dynamics and Earthquake Engineering* 16.7-8 (1997), pp. 495–502.

[17] Mathworks. *Cross-correlation*. 2006. URL: `https://se.mathworks.com/help/signal/ref/xcorr.html` (visited on 28/03/2017).

[18] Agilent Technologies. *The Fundamentals of Signal Testing*. 1999. URL: `http://cp.literature.agilent.com/litweb/pdf/5952-8898E.pdf` (visited on 08/02/2017).

[19] Analog Dialogue. *Practical Filter Design for Precision ADCS*. 2016. URL: `http://www.analog.com/en/analog-dialogue/articles/practical-filter-design-precision-adcs.html` (visited on 12/05/2017).

[20] Evans D. J. *Modal Testing: Theory and Practice*. Letchworth, England: Research studies press, 1984.

[21] Ben- Israel A. and Greville T. N. E. *Generalized Inverses*. Springer-Verlag, 2003.

[22] Agilent Technologies. *The Fundamentals of Modal Testing*. 2000. URL: `http://cp.literature.agilent.com/litweb/pdf/5954-7957E.pdf` (visited on 01/02/2017).

[23] Allemang R. J. 'The modal assurance criterion - twenty years of use and abuse '. In: *Journal of Sound and Vibration* 37.8 (2003), pp. 14–23.

[24] Abrahamsson T. *FEMcali*. Version 1.12. 31st Jan. 2017. URL: `https://se.mathworks.com/matlabcentral/fileexchange/44317-femcali`.

[25] Data Translation. *QuickDAQ*. Version 3.7.0.41. 21st Feb. 2017. URL: `https://www.mccdaq.com/Products/Data-Acquisition-Software/QuickDAQ`.

[26] Bengtsson H., SMHI. *Weather data Åmål*. 8th May 2017.

Appendices

A Mode Shapes

Figure A.1-A.11 show the mode shapes for the -70° set-up.

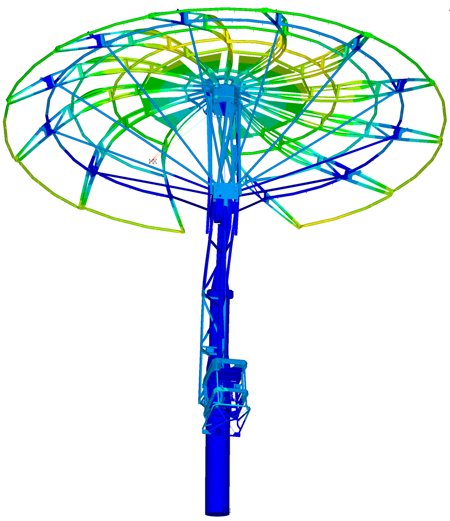

Figure A.1: 5th mode shape for -70° set-up.

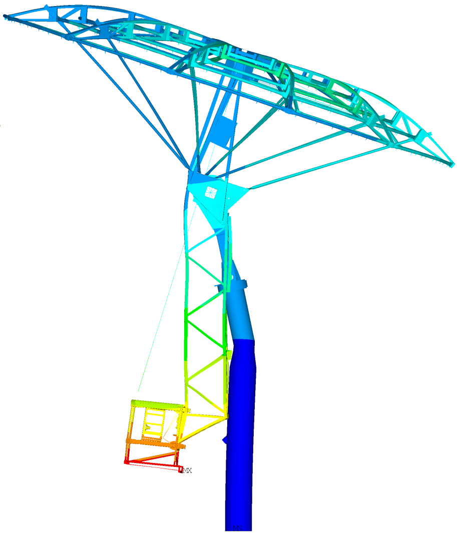

Figure A.2: 6th mode shape for -70° set-up.

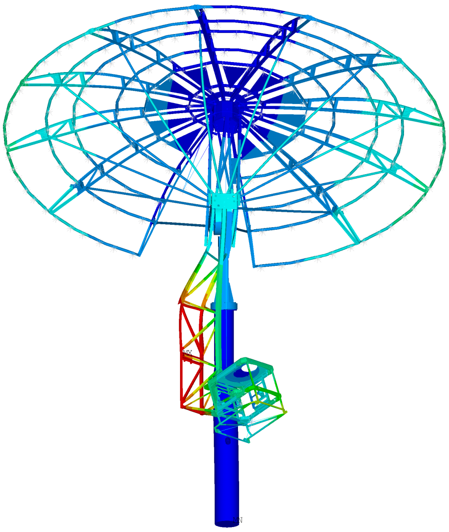

Figure A.3: 7th mode shape for -70° set-up.

Figure A.4: 8th mode shape for -70° set-up.

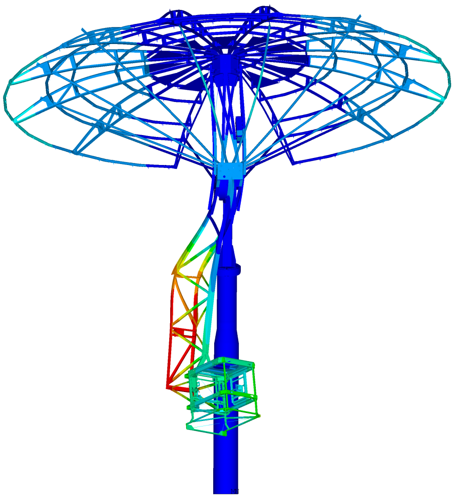

Figure A.5: 9th mode shape for -70° set-up.

Figure A.6: 10th mode shape for -70° set-up.

Figure A.7: 11th mode shape for -70° set-up.

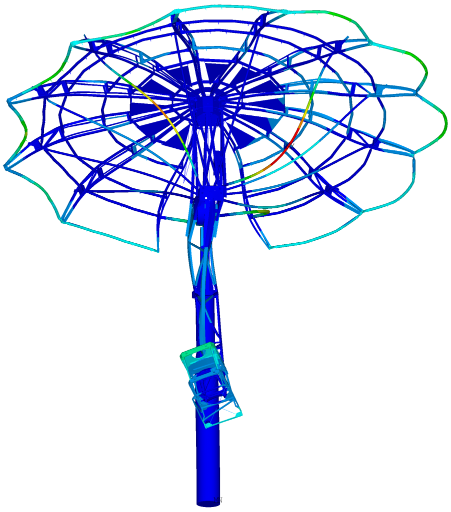

Figure A.8: 50th mode shape for -70° set-up.

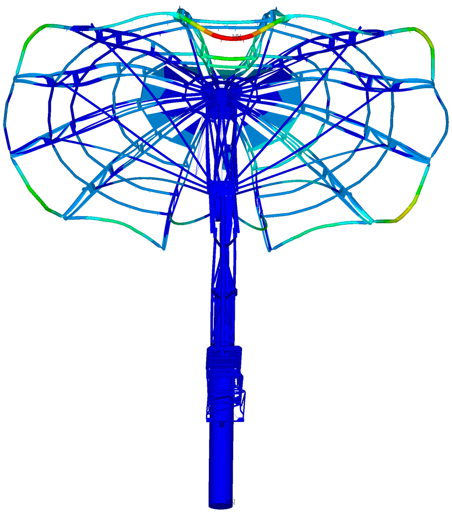

Figure A.9: 67th mode shape for -70° set-up.

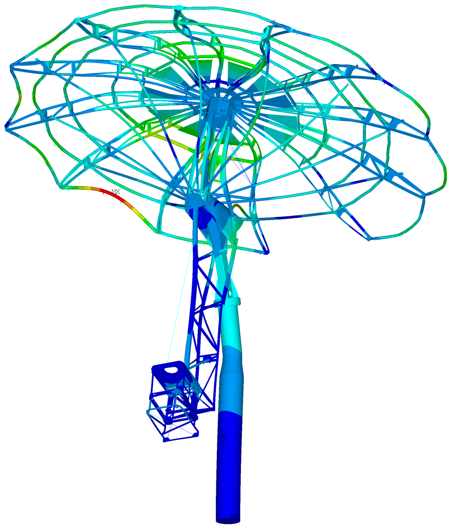

Figure A.10: 50th mode shape for -70° set-up.

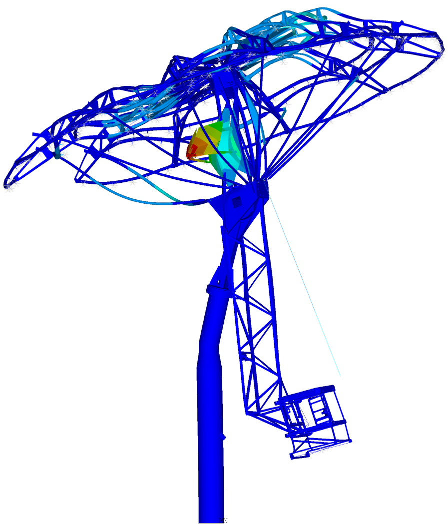

Figure A.11: 75th mode shape for -70° set-up.

B Aligned Signals

Figure B.12-B.18 show the selected and aligned blocks for the -70° set-up.

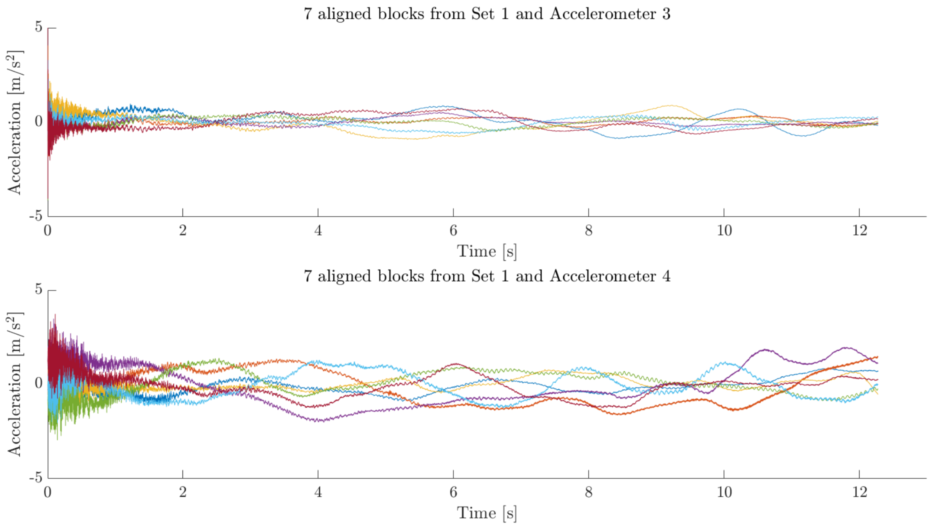

Figure B.12: Selected and aligned blocks from accelerometer 3 and 4 in set 1.

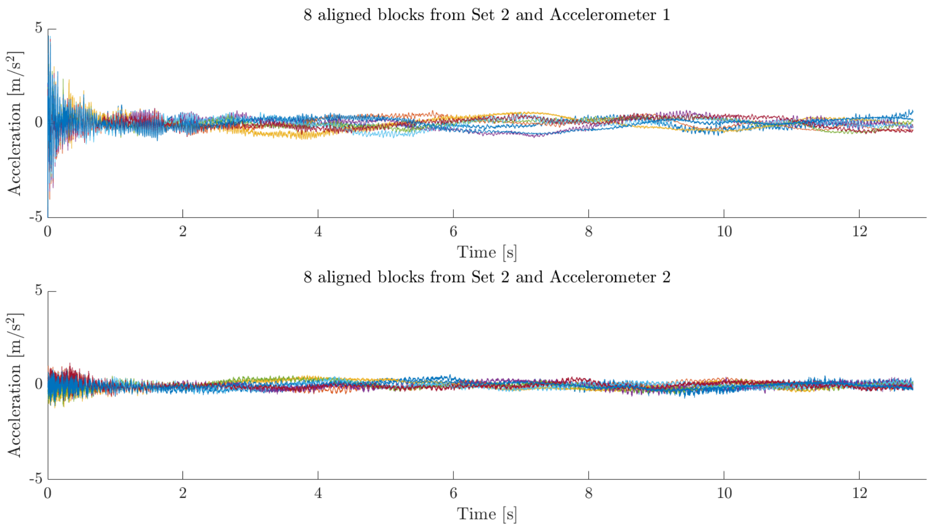

Figure B.13: Selected and aligned blocks from accelerometer 1 and 2 in set 2.

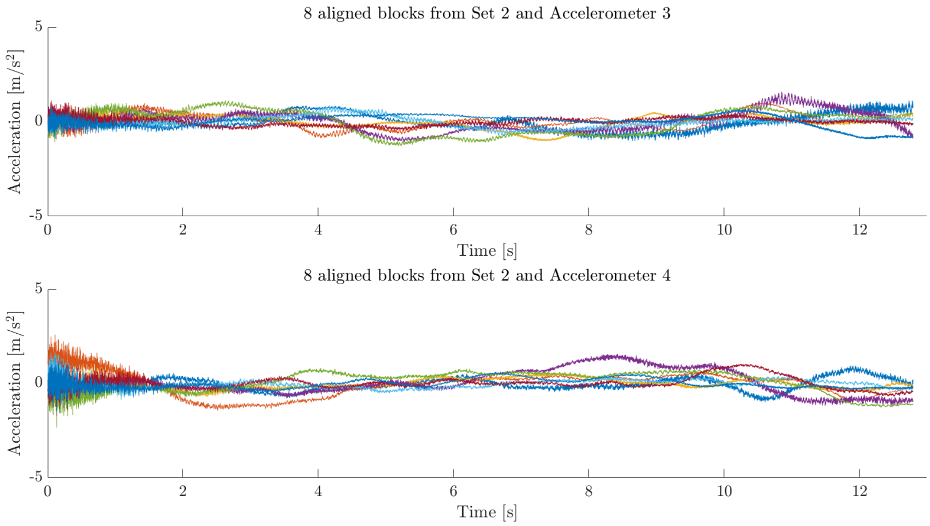

Figure B.14: Selected and aligned blocks from accelerometer 3 and 4 in set 2.

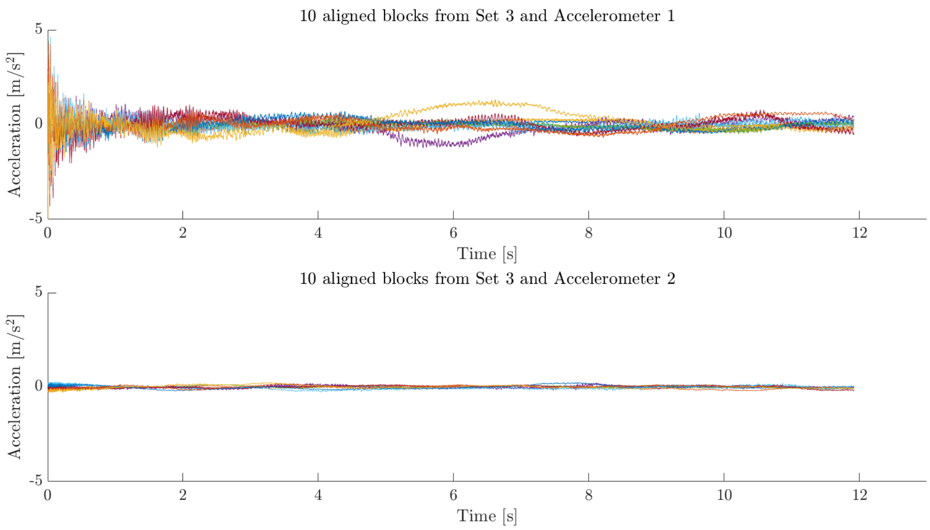

Figure B.15: Selected and aligned blocks from accelerometer 1 and 2 in set 3.

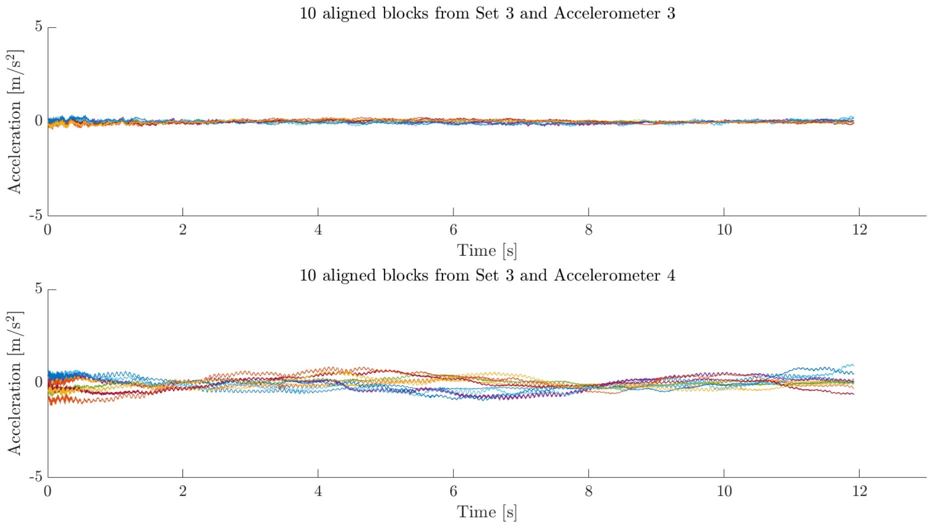

Figure B.16: Selected and aligned blocks from accelerometer 3 and 4 in set 3.

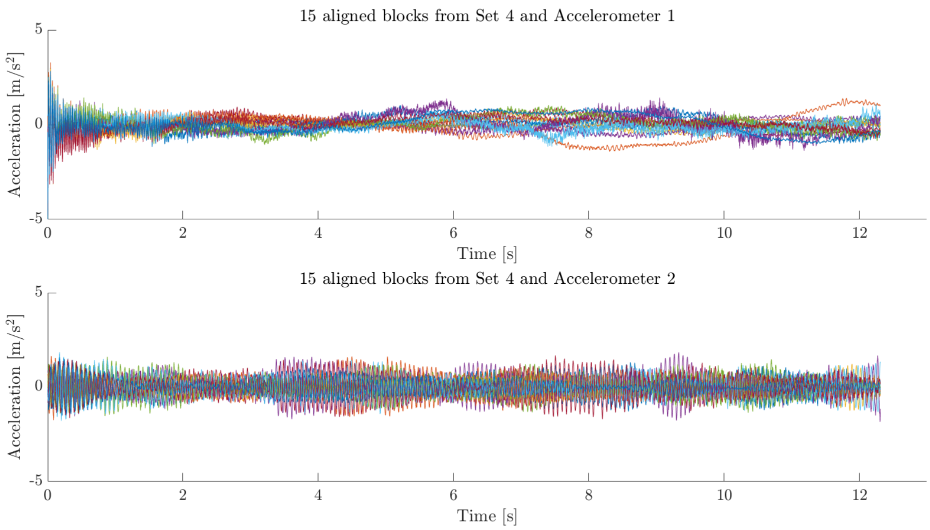

Figure B.17: Selected and aligned blocks from accelerometer 1 and 2 in set 4.

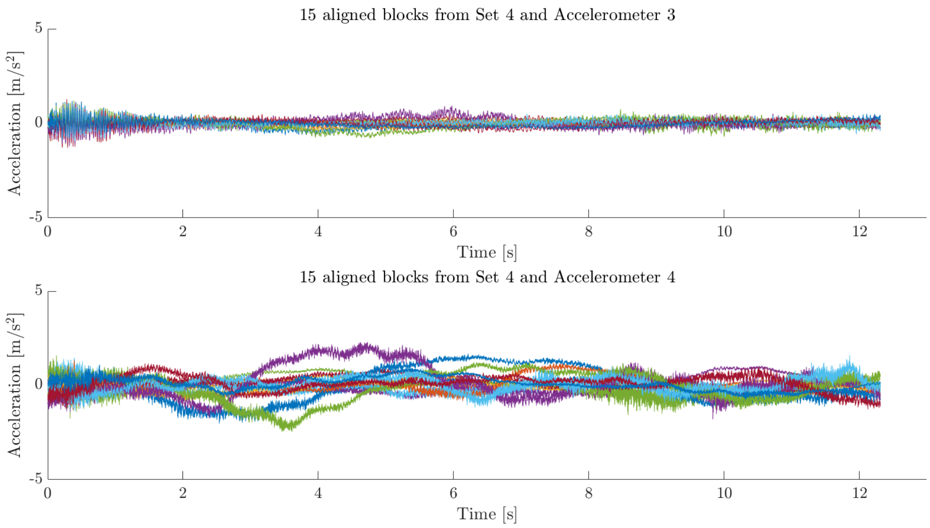

Figure B.18: Selected and aligned blocks from accelerometer 3 and 4 in set 4.